Development of Rational Combination Therapies for Patients with Metastatic Prostate Cancer and Loss of the PTEN Tumor Suppressor Gene

[Pimchanok Tipayasri]

Utrecht University
Cancer, Stem Cells & Developmental Biology

The Netherlands Cancer Institute
Division of Molecular Carcinogenesis

Assessor: Professor René Bernards
Supervisors: Koen van der Mijn & Robin Jansen
Examinor: Professor Sabine Linn

Table of Contents

1. Plain language summary

Metastatic castration resistant prostate cancer (mCRPC) is a deadly disease with no cure. The current treatments by blocking androgen signaling eventually do not work because of cancer cells that become resistant, often by increasing the amount of androgen receptor and its activity. In almost half of mCRPC patients, a tumor suppressor PTEN is lost, leading to an increased signaling in PI3K/AKT pathway that promotes tumor growth and survival. Drugs that block PI3K/AKT can be effective in patients with PTEN-loss mCRPC, but with a small clinical benefit because cancer cells can adapt and rely on other pathways as a compensation to survive. For example, breast cancer cells rely on MAP2K4 and become resistant to drugs that block PI3K. Researchers also showed that fueling the signaling pathways that are already highly active can kill cancer cells. This strategy is referred to as the overactivation of oncogenic signaling. Since the majority of PTEN-loss prostate cancer cells already exhibit highly active AKT pathway and AR signaling, deliberately activating these pathways even further may kill prostate cancer. Therefore, this study aims to find other drug combination that can improve the effectiveness of the AKT blocker called Ipatasertib. We also focused on developing new combination treatments that work specifically with overactivation of oncogenic signaling in PTEN-loss mCRPC. In our study, we conducted experiments to test the fitness of the cells when treated with potential drug combinations. We showed that Ipatasertib in combination with another drug called HRX-0233 which blocks MAP2K4 is synergistic, meaning that the combination is much more effective than the sum of their individual effects in prostate cancer cells that do not have androgen receptor. To gain a deeper understanding of this synergy, we investigated the levels of activated proteins in the relevant pathways, namely mTORC1 and MAPK pathway, and found that the combination can cooperatively inhibit both pathways more than the individual drugs. In search of other possible combinations, we performed so-called CRISPR knockout screen experiment where we turned off genes one by one and looked for cells that do not survive the treatments with Ipatasertib or HRX-0233. Our main findings revealed that cells without cyclin D1 are vulnerable to Ipatasertib. We confirmed this finding using Palbociclib, a drug that indirectly block the activity of cyclin D1 in combination with Ipatasertib. We showed that Palbociclib can minimally increase sensitivity to Ipatasertib in PTEN-null prostate cancer cells. Additionally, we performed another CRISPR knockout screen experiment to identify vulnerable targets to the overactivation of oncogenic signaling using the drugs called LB-100 and synthetic androgen R1881. LB-100 can promote activation of AKT pathway, while R1881 can promote AR signaling. Our results from the screen uncovered many candidate genes that when turned off can sensitize cells LB-100 and R1881. Overall, this research highlights the potential of combining Ipatasertib with HRX-0233 as a new therapy for AR-negative prostate cancer and identifies multiple genes that can be targeted when oncogenic signaling is hyperactivated.

2. Abstract

Metastatic castration resistant prostate cancer (mCRPC) is a lethal disease, as current treatments involving the inhibition of androgen signaling eventually lead to resistance mainly mediated by AR amplification and increased AR sensitivity to androgen. In 50% of mCRPC patients, tumor suppressor PTEN is lost which results elevated PI3K/AKT signaling. Previous research demonstrated clinical activity of AKT inhibitors specifically in PTEN-null mCRPC, however with a modest clinical benefit. Recently, the overactivation of oncogenic signaling has been proposed as an alternative strategy for cancer treatment, suggesting that overactivating AR signaling and AKT pathway can be lethal to prostate cancer cells. The objective of this study is to enhance the efficacy of the currently available AKT inhibitor Ipatasertib as well as to develop novel combination strategies to exploit the hyperactivation of the oncogenic pathways in PTEN-null mCRPC. In this study, we evaluated putative synergistic drug combination by cell viability assay and colony formation assay, as well as genome-wide CRISPR screens to identify potential novel treatment combinations. Our findings revealed that Ipatasertib is synthetic lethal with HRX-0233, a MAP2K4 inhibitor in AR negative prostate cancer regardless of PTEN status. At the molecular level, Ipatasertib and HRX-0233 cooperatively impaired the mTORC1 signaling as well as c-Jun and cyclin D1. Furthermore, genome-wide CRISPR screen identified the loss of cyclin D1 as a vulnerability in prostate cancer cells undergoing treatment with Ipatasertib. We validated this observation using clinically available CDK4/6 inhibitor Palbociclib to disrupt signaling of the CDK4/6-cyclin D1 complex. The combination of Ipatasertib and Palbociclib demonstrated an additive effect on cell viability. We also identified the loss of multiple mitotic spindle components that sensitize castration resistant PTEN-null cells to overactivation of oncogenic signaling by LB-100, as well as multiple vulnerable targets to the treatment with supraphysiological levels of synthetic androgen R1881.

Overall, this study highlights the potential of Ipatasertib based combination treatments with HRX-0233 novel therapeutic strategy in AR-negative prostate cancer. We also found that cyclin D1 is a vulnerable target to Ipatasertib, but that pharmacological validation showed inferior efficacy to Ipatasertib and HRX-0233 combination. Finally, we identified various targets which are susceptible to the overactivation of oncogenic signaling that should be considered when exploring alternative therapeutic strategy for PTEN-null castration resistant prostate cancer.

3. Introduction

3.1 Metastatic castration resistant prostate cancer

Prostate cancer ranks second in the most commonly diagnosed cancer among men worldwide, with approximately 1.4 million new cases and nearly 400.000 deaths in 2020 [1,2]. Since the majority of prostate cancer is driven by activation of androgen signaling, suppressing androgen signaling by androgen-deprivation has remained the first-line treatment for prostate cancer. Despite initial response, this therapy eventually fails to impede cancer progression due to acquired resistance. This advanced stage of the disease accompanied by the development of metastases is referred to as metastatic castration resistant prostate cancer (mCRPC). Until present days, there is no curative treatment for mCRPC and new therapeutic strategies are urgently needed.

3.2 Loss of PTEN tumor suppressor and activation of AKT are associated with poor clinical outcome

mCRPC is associated with loss of tumor suppressor genes. Phosphatase and tensin homolog (PTEN) is reported to be the most frequently lost tumor suppressor that occurs in 20% of primary prostate cancer and the incidence is increased to 50% in mCRPC. PTEN is a critical negative regulator of the phosphatidylinositol-3-kinase (PI3K) pathway. PI3K initiates downstream signaling cascade by synthesizing the secondary messenger phosphatidylinositol 3,4,5 triphosphate (PIP3) from phosphatidylinositol 4,5 bisphosphate (PIP2). PIP3 promotes the phosphorylation and activation of the kinase AKT (also known as protein kinase B or PKB). Once active, AKT phosphorylates a number of substrates that ultimately promote cancer cell growth, proliferation and tumor survival. PTEN blocks the AKT activation by converting PIP3 back to PIP2, and its loss facilitates sustained activation of AKT. Previous research has shown that PI3K pathway and androgen signaling can cross-regulate each other by reciprocal feedback [3,4,5]. The activation of AR signaling results in the inhibition PI3K pathway. Conversely, the activation of PI3K pathway results in the AR signaling blockade. Subsequently, the loss of PTEN and persistent activation of PI3K/AKT signaling cascade drive the tumor transition towards the AR-independent state and is therefore highly correlated with reduced response to ADT and unfavorable prognosis.

3.3 AKT inhibitor-based combination therapies

Several PI3K/AKT inhibitors are in clinical development that are able to target all three AKT isoforms (i.e., AKT1, AKT2 and AKT3). The single-agent AKT inhibitors yield limited clinical benefits and are often associated with low tolerability [6, 37]. The modest efficacy of monotherapies in prostate cancer provides a strong rationale to investigate combination therapies. As recently investigated in a phase III trial, dual pathway inhibition with Ipatasertib, an ATP-competitive pan-AKT inhibitor plus androgen synthesis inhibitor Abiraterone demonstrated a prolonged median progression free survival (PFS) specifically in mCRPC patients with PTEN-loss mutation compared to the monotherapy Abiraterone (median 18.5 vs. 16.5 months) [7]. Similarly, a randomized phase II clinical trial showed clinical benefit of the pan-AKT inhibitor Capivasertib plus Docetaxel in mCRPC patients (median PFS of 7.03 vs. 6.70 months) [8]. While these clinical results demonstrated the activity of AKT inhibitors in mCRPC patients and a pronounced benefit of Ipatasertib in PTEN-null subgroup, they also emphasize the clinical need for more effective combinations.

3.4 Role of MAP2K4 in prostate cancer

The efficacy of AKT inhibitors as monotherapy is often limited by acquired resistance, as cancer cells have the ability to rewire cellular signaling to activate feedback mechanisms and alternative pathways to compensate for the inhibition of AKT. The mitogen-activated protein kinase (MAPK) pathway is believed to play an important role, as it being the key signaling hub integrating extracellular signals for the control of cell proliferation and survival. The PI3K/AKT and MAPK pathway are interconnected at multiple levels, owing to shared upstream activation through receptor tyrosine kinase (RTKs) [9]. Mitogen-activated protein kinase 4 (MAP2K4, also known as MEK4, MKK4 and SEK1) is a component of stress-activated MAPK pathway, and its overexpression correlates with the development of metastasis in prostate cancer [10]. Importantly, previous study in triple negative breast cancer demonstrated that the activity of MAP2K4 by phosphorylation is upregulated upon PI3K inhibition and that knockdown of MAP2K4 has shown to increase sensitivity to PI3K inhibitors [11]. Additionally, treatment with PI3K inhibitor Buparlisib resulted in a much lower level of phosphorylated AKT, and its downstream target phosphorylated ribosomal protein S6 (p-S6) in MAP2K4 knock down cells compared to the control cells. Therefore, it is plausible that cancer cells rely on MAP2K4 to compensate for the inhibition of the PI3K pathway. However, the role of MAP2K4 and its relationship with the PI3K pathway in prostate cancer remains unexplored and should be further elucidated, possibly as a co-target in PI3K/AKT combination therapy.

3.5 Overactivation of oncogenic signaling as an alternative treatment for prostate cancer

Opposing to conventional strategies to inhibit oncogenic signaling, overactivation of oncogenic signaling has emerged as an alternative approach to treat cancer. As mitogenic signaling is highly active in cancer cells, stress response pathway is activated to maintain homeostasis. Previous findings revealed that overactivating oncogenic pathways can be lethal to cancer cells [12]. It has been reported inhibition of protein phosphatase 2A (PP2A) hyperactivates numerous oncogenic pathways including PI3K/AKT signaling. Building on this concept, overactivating PI3K/AKT signaling by inhibiting PP2A could increase sensitivity in PTEN-loss prostate cancer to anti-cancer drugs, potentially to compounds targeting stress response pathway. Another evidence supporting the principle of overactivation of oncogenic signaling is that exogenous androgen is shown to suppress growth in prostate cancer cells [14], contradicting the foundation of androgen deprivation therapy. Particularly, castration resistant prostate cancer adaptively upregulates AR activity via mechanisms such as AR overexpression and amplification, increasing its vulnerability to supraphysiologic androgen [37]. It is reported that high dose of synthetic androgen (R1881) leads to downregulation of the oncogene c-MYC and therefore induces tumor regression [15, 16, 17]. R1881 has been investigated in clinical studies, as a part of bipolar androgen therapy (BAT). BAT consists of periodical oscillation between castration levels and supraphysiological levels of androgen [18]. Results of phase I and II clinical trials have shown that lower levels of prostate specific antigen (PSA) are significantly decreased in treated mCRPC patients [19,20] These findings indicate that prostate cancer cells may be sensitive to the overactivation of AR and AKT signaling. Therefore, overactivation of AR and AKT signaling could provide novel therapeutic strategy for PTEN-null mCRPC.

3.6 Aim of the study

In this research project, we set out to develop novel combination therapies for patients with PTEN-null prostate cancer. We aim to enhance the efficacy of the currently available AKT inhibitor Ipatasertib as well as develop innovative novel combination strategies based on the concept of hyperactivation of the most frequently activated oncogenic pathways in mCRPC.

4. Material and methods

4.1 Reagents

Pan-Akt inhibitor (Ipatasertib, GDC-0688, 10 mM in DMSO, Selleckchem, # S2808), MAP2K4 inhibitor (HRX-0233, 10 mM in DMSO, Heparegenix), synthetic androgen (R1881, 10 mM in DMSO, a kind gift from Wilbert Zwart), PP2A-inhibitor (LB-100, 5 mM in DMSO, MedKoo, #206834). CDK4/6 inhibitor (Palbociclib, PD-0332991, 5mM in DMSO, Medkoo, #123215)

4.2 Cell culture and generation of Cas9 expressing cell lines

The human prostate cancer cells PC3, LnCap-abl, LnCap, DU145, LuCap 184.9, LuCap 35CR, LuCap 179) were provided by the Netherlands Cancer Institute. PC3, LnCap, DU145 cells were cultured in RPMI-1640 supplemented with 10% FBS, 2 mmol/L L-glutamine and 1% penicillin/streptomycin (Gibco). LnCap-abl cells were cultured in RPMI-1640 supplemented with 10% charcoal stripped FBS (v/v), 2 mmol/L L-glutamine and 1% penicillin/streptomycin. Castration-resistant signature of LnCap-abl was confirmed based on its resistance to enzalutamide. LuCap 189.4, LuCap 35CR, LuCap 179 cells were a kind gift from Wilber Zwart. All LuCap cell lines were cultured in DMEM supplemented with 10% FBS (v/v), 2 mmol/L L-glutamine and 1% penicillin/streptomycin. All cells were maintained at 37 °C in 5% CO_2. All cells were routinely tested for absence of mycoplasma infections by PCR. We confirmed the identity of PC3 cells by STR profiling.

Cas9 expressing PC3 and LnCap-abl cell lines were generated by viral transduction of lentiCas9-blast vector (Addgene #52962), enhanced with 8 µg/mL polybrene. Infected cells were selected with 10 µg/mL blasticidin for 7 days or until the uninfected control cells were eliminated.

4.3 Flowcytometry

The expression of Cas9 in was analyzed by flowcytometry. Infected cells were trypsinized and centrifuged at 300 RCF. Cell pellets were washed with phosphate-buffered saline (PBS), fixed with 4% formaldehyde and permeabilized with ice-cold 100% methanol. Cell pellets were incubated in 1:100 mouse anti-Cas9 antibody diluted in PBS supplemented with 0.5% BSA for 1 h on ice, followed by 3 washing steps with PBS supplemented with 0.5% BSA. Next, cell pellets were incubated in 1:500 anti-mouse Alexa 647 antibody diluted in PBS supplemented with 0.5% BSA for 15 min in the dark. After 3 washing steps, the cells were resuspended and subjected for flowcytometry. The expression of Cas9 is determined by comparing the fluorescent signal from Alexa fluor 647 of the infected population with the non-infected control.

The Cas9 editing efficiency was also quantified by flowcytometry. Cells expressing Cas9 were infected with lentivirus to deliver mCherry, BFP and sgRNA targeting BFP (Addgene, #67686), so that successfully edited cells would express mCherry but not BFP. Cells expressing Cas9 infected with lentivirus containing sequences for mCherry, BFP and a non-targeting sgRNA (Addgene, #67685) were included as a negative control. 1 Day after the infection, cells were fixed and subjected for flowcytrometry. All flowcytometry data were analyzed using FlowJo v10.8.2.

4.4 Library amplification and virus production

200 ng of plasmids containing Human CRISPR Knockout Pooled Library (Brunello) in LentiCRISPRv2 backbone (Addgene #73179) were introduced into 100 µL electrocompetent *Escherichia coli* (Endura). Bacterial suspension was aliquoted into 4 separate 0.1 cm-gap cuvettes, followed by an electroporation at 1.8 kV. The electroporated cells were pooled, resuspended in SOC medium (New England Biolabs) and incubated in a shaking incubator at 250 rpm for 1 hour at 37 °C. The bacteria were then plated onto

a total of 19x 15 cm agar plates containing 100 mg/mL Carbenicillin (Fisher Scientific) to maintain the genome–wide library representation and to select for successful transformants. The agar plates were incubated overnight at 37 °C. All formed colonies were harvested on the following day. The library plasmid DNA was isolated using the Purelink HiPure Plasmid Filter Maxiprep kit (#K210016) according to the manufacturer's protocol.

Lentivirus components were amplified as preparation for lentiviral library production. 2nd generation packaging plasmids psPAX2, (Addgene #12260) and VSV-G envelope expressing plasmids (pMD2.G, #Addgene #12259) were used to transform chemically competent cells following the manufacturer's recommendation (DH5α, Thermo Fisher Scientific). The plasmid DNA was isolated as previously mentioned.

The lentiviral particles were generated by co-transfection of the psPAX2, pMD2.G and the transfer plasmids in Lenti-X 293T cells facilitated by 8 µg/mL polybrene. 2 $*10^6$ Lenti-X 293T cells were seeded in a 15 cm dish. The transfection mixture consisted of 6 µg transfer plasmid DNA, 2.25 µg psPAX2 and 0.75 µg pMD2.G in 800 µL OptiMEM. Polyethyleneimine (PEI max, Polysciences) was added to the mixture so that the DNA:PEI MAX ratio was 1:5. The solution was incubated at room temperature for 20 min and subsequently transferred to Lenti-X 293T cells. The cells were incubated overnight at 37 °C, 5% CO_2. The viral supernatant was collected 48h post transfection and was filtered with 0.4 µM syringe filter, snap-frozen in liquid nitrogen and stored at -80 °C.

4.5 Genome wide CRISPR-Cas9 dropout screens

Population of 1.30$*10^7$ PC3-cas9 expressing cells were infected with 2 vector system CRISPR Knockout Pooled Library (Brunello) in lentiguide-puro backbone (Addgene #73178). 3.3$*10^7$ LnCap-abl-Cas9 expressing cells were infected with 1 vector system Human CRISPR Knockout Pooled Library (Brunello) in LentiCRISPRv2 backbone (Addgene #73179). The infection is facilitated by 8 µg/mL polybrene at multiplicity of infection (M.O.I) = 0.3 aiming for single viral integration per cell, and at a 375-fold coverage of the genome-wide library. 24 Hours after transduction, cells were selected for guide integration with 2 µg/mL puromycin for 3 days. Cells harboring sgRNA were seeded in 15 cm dishes (the seeding density was 1.5$*10^6$ for PC3 cells and 2 $*10^6$ for LnCap-abl). PC3 cells were cultured in 2 µM Ipatasertib, or 4 µM HRX-0233 for 2 weeks and were propagated every 4-5 days and reseeded at a density of 1.5$*10^6$ cells per dish. LnCap-abl-Cas9 were allowed to attach to the culture dish and to recover for 3 days prior to the treatment with 5 nM R1881 or 1 µM LB-100. LnCap-abl cells were propagated every 7 days and media refreshed every 3-4 days. 30 $*10^6$ cells were collected following sgRNA integration (T_0 control). For both screens, 3 replicates were accounted for all conditions. After 10 cell doublings, 15 $*10^6$ cells of each replicate and treatment groups were collected in duplicate to maintain representation of the Brunello library. Cell pellets were snap-frozen on dry ice and stored at -80 °C, from which DNA was isolated using Gentra Puregene Cell Core Kit (QIAGEN, 172025287).

4.6 Preparation of the sequencing library from genomic DNA

Upon obtaining genomic DNA, the lentiviral integrants containing the sgRNA sequence were enriched by restriction digestions using NdeI and PstI-HF restriction enzymes for 2 vector system CRISPR-KO system, and NdeI and XbaI restriction enzymes for 1 vector CRISPR-KO system. Next, digested DNA fragments were denatured and hybridized with biotinylated oligos, facilitated by 2M NaCl. Biotin-probed sgRNA sequences were then captured with Streptavidin T1 Dynabeads, followed by 2 washing steps with wash buffer (10 mM Tris-HCl, pH 8) in 10 M NaCl using DynaMagTM-2 magnet rack to remove excess genomic DNA. The samples were then washed 3 times with the wash buffer and incubated with Exonuclease I (20U, New England Biolabs, # M0293L) in 1x Exonuclease buffer and 10 mM Tris-HCl for 1h at 37 °C to digest unannealed oligos. Finally, the samples were washed 3 times, resuspended in the wash buffer, and stored at 4 °C.

As preparations for sgRNA recovery, unique barcodes were added to the samples by PCR to allow pairing of sequenced reads with the corresponding condition of the screen (Supplementary figure 2). PCR products of each replicate reaction were pooled and used for the second PCR, introducing p5 and p7 adapters required for the annealing to the Illumina flow cell, as well as an additional barcode sequence.

The final PCR products were purified using Bioline ISOLATE II PCR purification kit according to the manufacturer's instructions. The DNA concentrations of each condition were quantified by Qubit and submitted equimolarly for sequencing by Illumina HiSeq 2500 genome analyzer at the Genomics Core Facility (NKI).

4.7 Cell viability assay

The effect of the drugs on cell viability of various prostate cancer cell lines was assessed by cell titer blue assay. Cell lines were seeded into 384-well plates with a seeding density per well of 500 for PC3 and DU145, 2000 for LnCap and LnCap-abl and 3000 for LuCap 189.4, LuCap 176 and LuCap 35CR. After 24h incubation, drugs were added to final drug concentration ranging from 0.026-20 µM. (Ipatasertib in PC3 & DU145 cell lines), 2.6 nM-2 µM (Ipatasertib in other cell lines) 0,2-20 µM (HRX-0233 and Palbociclib). Cells treated with 10 µM phenylarsine oxide (PAO, Sigma, #637-03-6) served as a positive control. Untreated cells served as a negative control. 6 Days after treatment, culture media were refreshed with media containing Resazurin (Sigma, #R7017), followed by an incubation for 3 h at 37°C in 5% CO_2. Absorbance was measured using the Envision 2104 Multilabel Reader (PerkinElmer). The relative viability of treated cells was calculated after normalizing the absorbance of treated cells against untreated cells after subtraction of background fluorescence.

4.8 Protein lysate preparation and Western Blot

Cells were plated 24 h prior to the drug treatments. At the time of harvest, cells were washed with ice-cold PBS and lysed with RIPA buffer (25 mM Tris-HCl, pH 7.6, 150 mM Nacl, 1% NP-40, 1% sodium deoxycholate, 0.1% SDS) supplemented with protease and phosphatase inhibitor cocktails (Sigma). Cell lysates were centrifuged at 14.000 x g at 4°C for 30 min to remove cellular fragments. Protein concentration was determined and normalized using BCA assay and Pierce™ BCA Protein Assay Kit (Thermo Fisher Scientific). 1x NuPAGE LDS Sample Buffer 1x and Sample Reducing Agent (Thermo Fisher Scientific) were added to the protein samples. Next, the protein samples were denatured by incubation at 100 C for 10 min. Equal amount of proteins were separated by SDS-PAGE (Bolt Bis-Tris Plus Thermo Fisher Scientific) in 4-12% polyacrylamide gels at 100V for 1 h 45 min and transferred to nitrocellulose membranes 0.45 µm (Amersham™ Protran™) at 350 mA for 2 h. The blotting membranes were then blocked with 5% BSA diluted in TBS-T (10 mM Tris, 150 mM NaCl, 0.1% Tween-20, pH 7.5) on a shaker for 1 h at room temperature, followed by an overnight incubation with the primary antibodies diluted 1:1000 in 5% BSA at 4°C. The blotting membranes were washed 3 times with TBS-T buffer for 10 min each time to remove unbound antibodies. Subsequently, the blotting membranes were probed with the secondary antibodies (HRP conjugated) diluted 1:10000 in 5% BSA for 1h at room temperature, followed by 3 washing steps with TBS-T. The protein bands were stained with Clarity™ Western ECL Substrate (Bio-Rad) to be visualized by chemiluminescence. Finally, the blotting membranes were imaged by ChemiDoc Imaging System (Bio-rad). Vinculin and α-tubulin were used as loading controls. The molecular weight of proteins was verified with Spectra™ Multicolor Broad Range Protein Ladder (Thermo Fisher Scientific). A complete list of used primary antibodies is provided below.

Table 1: List of primary antibodies, including the catalog number, the source, and the host.

Antibody	Host	Clonality	Clone	Manufacturer	Catalog no.
AR	Rabbit	Polyclonal		Cell signaling Technology	#3202
PSA	Rabbit	Monoclonal	D6B1		#5365
PTEN	Rabbit	Polyclonal			#9552
Phospho-Akt (Ser473)	Rabbit	Monoclonal	D9E		#4060
Phospho-Akt (Thr308)	Rabbit	Monoclonal	D25E6		#13038
Akt (pan)	Mouse	Monoclonal	40D4		#2920
S6 Ribosomal Protein	Rabbit	Monoclonal	5G10		#2217
S6 Ribosomal Protein (Ser235/236)	Rabbit	Polyclonal			#2211
S6 Ribosomal Protein (Ser240/244)	Rabbit	Monoclonal	D68F8		#5364
4EBP1	Rabbit	Monoclonal	53H11		#9644
Phospho-4EBP1 (Ser65)	Rabbit	Monoclonal	174A9		#9456
Phospho-4EBP1(Thr37/46)	Rabbit	Monoclonal	236B4		#2855
Phospho-MAP2K4 (Ser 257)	Rabbit	Monoclonal	C36c11		#4514
MAP2K4	Rabbit	Polyclonal			#9152
Phospho-c-Jun (Ser73)	Rabbit	Monoclonal	D47G9		#3270
c-Jun	Mouse	Monoclonal	L70B11		#2315
Cyclin D1	Rabbit	Monoclonal	92G2		#2978
Phospho-RSK	Rabbit	Monoclonal	D1E9		#8735
RSK	Rabbit	Monoclonal	D6D5		#8408
Alpha-tubulin	Mouse	Monoclonal		Sigma Aldrich	#T9026
Vinculin	Mouse	Monoclonal			#V9131

4.9 Colony formation assay

PC3 cells were seeded at low density in 24-well plates (Greiner Cell®). On the following day, the drugs were added using a Tecan D300e digital dispenser. Media containing drugs were refreshed every 3-4 days. Once the untreated controls were confluent, the cells were fixed with 4% formaldehyde (Millipore, #104002) diluted in PBS for 1h and stained with 0.1% crystal violet (Sigma, #HT90132) diluted in PBS. Usually after 1 day of staining, the plates were washed with demi water, left to air dry and imaged by EPSON v700/V750 scanner.

5. Results

5.1 Investigation of the combination therapy with AKT and MAP2K4 inhibitors

5.1.1 PC3 cells showed highest resistance to Ipatasertib among PTEN-deficient prostate cancer models

The first part of our study focused on optimizing Ipatasertib combination treatment for PTEN-null mCRPC patients. In search of a suitable model that represents this subgroup, we first characterized the activation of AR and PI3K signaling in available prostate cancer cell lines based on the expression of AR, PSA, PTEN, AKT, and phosphorylated AKT by Western blotting (Figure 1A). The analysis displayed undetectable levels of AR in DU145, PC3, LuCap 176 cell lines, while a distinct band was observed in LnCap, LnCap-abl and LuCap-35CR cell lines. PSA is a downstream of AR signaling and is used here as a readout for AR activity. PSA levels in LnCap and LuCap-35CR cell lines correspond with the expression of AR. In line with previous findings [21,22], LnCap-abl which is generated by long term androgen ablation of LnCap did not show clear expression of PSA despite being positive for AR, suggesting that LnCap-abl did not depend on AR activity to proliferate. Regarding PI3K signaling axis, PTEN was undetected in all cell lines with the exception of DU145. As expected, non PTEN expressing cell lines PC3, LnCap, LnCap-abl and LuCap 176 showed elevated levels of p-AKT when compared to DU145 cells. In short, we have identified 5 PTEN-deficient cell lines of which PC3, LnCap-abl and LuCap 176 are AR-independent, while LnCap and LuCap-35CR are AR-dependent.

Subsequently, we analyzed MAP2K4 signaling in these cell lines, as MAP2K4 is shown to mediate resistance to PI3K/AKT inhibition in triple negative breast cancer cell lines [11]. Western blot analysis showed differential MAP2K4 expression levels between cell lines. Previous research has identified 2 isoforms of MAP2K4, the canonical isoform of 44 kDA and a δ-variant of 41 kDA [23]. It was shown that both isoforms were able to activate downstream target p38 and JNK by phosphorylation. DU145, LnCap, LnCap-abl and LuCap 35CR showed two distinct bands corresponding to the molecular weights of the isoforms, indicating that both MAP2K4 and MAP2K4δ are expressed in these cell lines. Interestingly, PC3 and LuCap176 exhibited only one detectable band at 44 kDA, suggesting that these cell lines mainly expressed canonical MAP2K4. MAP2K4 requires phosphorylation to become active. The phosphorylation of the serine 257 residue is essential for its initial activation, but the phosphorylation of the threonine 261 residue is needed for its full activation [39]. Concomitant with the basal expression of MAP2K4, we observed various levels of phosphorylated MAP2K4 between cell lines. Overall, we observed a low level of p-MAP2K4 in PC3 and LnCap-abl in comparison to other cell lines.

To investigate the response of cell lines to Ipatasertib, viability assays were performed. Here, it was evident that the effects of Ipatasertib on cell viability widely differed between cell lines (Figure 1B). These results demonstrated that PC3 cells were the most resistant to Ipatasertib among PTEN-deficient cell lines (IC50 ± 13.00 μM, R^2 = 0.89), followed by LuCap 189.4 (IC50 ± 0.64 μM, R^2 = 0.64), LuCap 35CR (IC50 ± 0.32 μM, R^2 = 0.97), LnCap (IC50 ± 0.26 μM, R^2 = 0.97), LuCap 176 (IC50 ± 0.18 μM, R^2 = 0.97), whereas LnCap-abl cells were the most sensitive (IC50 ± 0.06 μM, R^2 = 0.97). The PTEN-expressing line DU145 showed an extremely high IC50 of 71.28 μM (R^2 = 0.68). In line with previous preclinical data [24], our results demonstrated that Ipatasertib had larger effects in PTEN-deficient than in PTEN-expressing cell line.

Collectively, PC3 has shown to be PTEN-deficient with high activation of AKT, AR-independent and Ipatasertib resistant. Therefore, we considered PC3 to be the most suitable cell line that best represents mCRPC patients with poor response to ADT and Ipatasertib treatment.

Based on the rationale that MAP2K4 could potentially be co-targeted in Ipatasertib combination treatment, we also performed viability assays to evaluate response of HRX-0233, a novel MAP2K4

inhibitor, in our cell line panels. Our results demonstrated that the effects of HRX-0233 on cell viability were similar in all cell lines, and that relatively high doses of HRX-0233 were required to induce changes in cell viability. PC3 cell line was once again the most resistant to HRX-0233 (IC50 ± 47.53; R^2 = 0.61), followed by DU145 (IC50 ± 14.78 µM, R^2 = 0.78), LnCap (IC50 ± 11.25 µM, R^2 = 0.79), LnCap-abl (IC50 ± 14.05 µM, R^2 = 0.82), LuCap 189.4 (IC50 ± 11.25 µM, R^2= 0.48), LuCap176 (IC50 ± 12.27 µM, R^2 = 0.88), and LuCap 35CR (IC50 ± 31.56 µM R^2 = 0.64). These results suggest that HRX-0233 had minimal effect on the viability of prostate cancer cells.

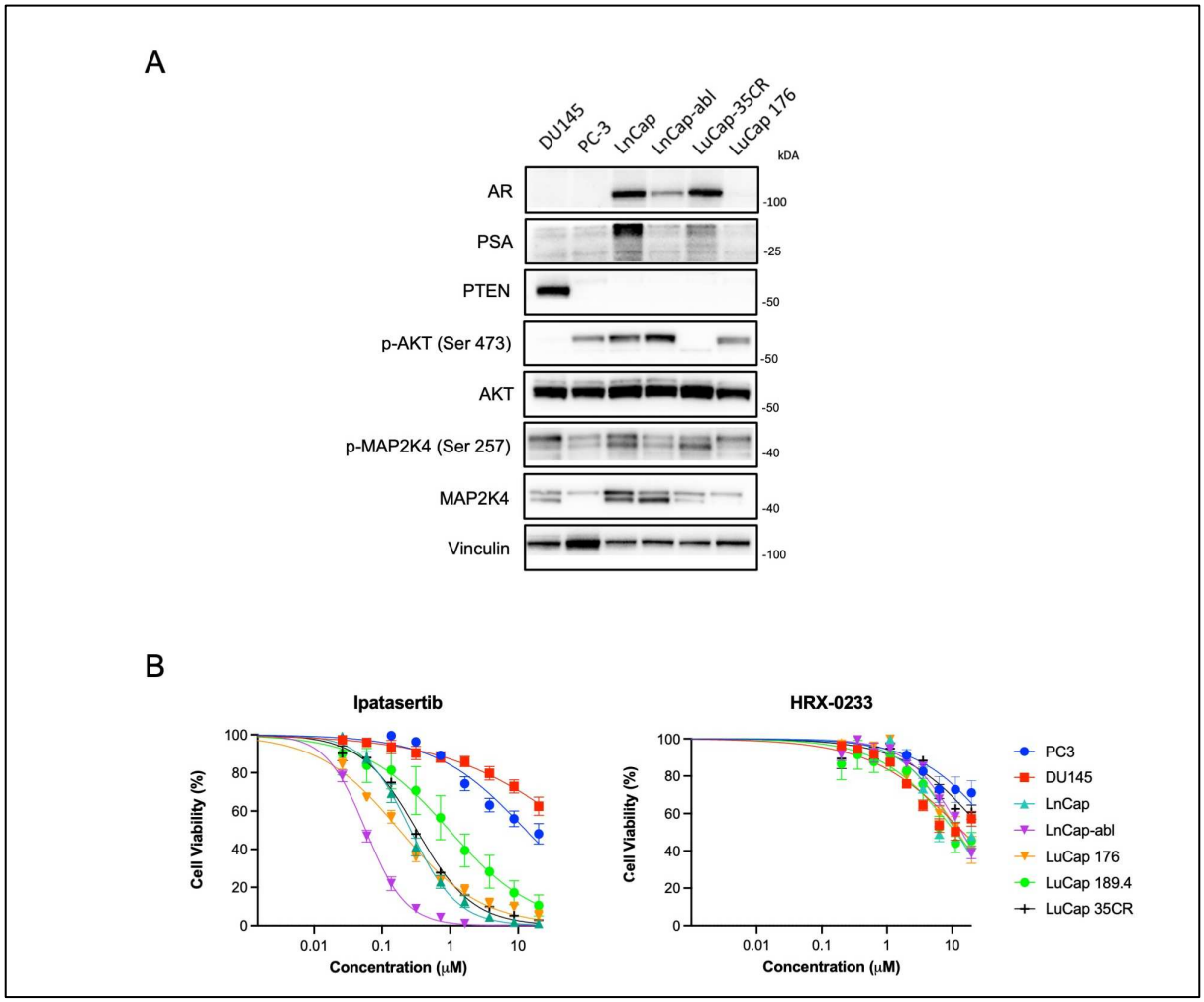

Figure 1: Characteristics of prostate cancer cell lines and drug responses. (A) Western blot showed basal expression of AR, PSA, PTEN, p-AKT, p-MAP2K4 and MAP2k4 in available prostate cancer cell lines DU145, PC3, LnCap, LnCap-abl, LuCap-35CR and LuCap 176. Vinculin served as loading control. Dose-response curves of prostate cancer cell lines under treatment with Ipatasertib or HRX-0233. (B) The values were normalized to PAO treated cells (positive control, 0% viability), and to non-treated cells (negative control, 100% viability). Error bars represented SEM. N = 3 independent experiment for each cell line.

5.1.2 Synergy between Ipatasertib and HRX-0233 in prostate cancer cell lines

High resistance found in PC3 cells gave rise to the question how Ipatasertib resistant cells modulate drug response. To investigate whether the activation of MAP2K4 is promoted in response to Ipatasertib in prostate cancer cells, we performed western blotting to compare the level of p-MAP2K4 in Ipatasertib treated and untreated PC3 cells. Indeed, PC3 cells treated with 2 μM and 4 μM Ipatasertib exhibited increased level of phosphorylated MAP2K4 within 6 hours (Figure 2A). The total level of MAP2K4 remained stable regardless of the treatment. Our results demonstrated that PC3 cells increased activation of MAP2K4 in response to Ipatasertib.

To determine whether the activation of MAP2K4 reduces the efficacy of Ipatasertib, we evaluated the efficacy of combination treatment. We started with long-term colony formation assays in PC3 cells using Ipatasertib and HRX-0233. We observed that particularly the combination of Ipatasertib and HRX-0233 had a large inhibitory effect on colony formation compared to monotherapy of either compound (Figure 2B).

Next, we determined the synergy between Ipatasertib and HRX-0233 combination in our cell line panel. A viability experiment was performed using the matrix concentrations and the ZIP synergy score was calculated. A ZIP score above 10 is considered synergy. Here we found that the combination of Ipatasertib and HRX-0233 was synergistic in PC3 cells with a ZIP synergy score of 11.573 (Figure 2C). The highest synergy in PC3 cells was observed at the concentrations of ± 0.7 μM Ipatasertib ± 3.6 μM HRX-0233. In DU145, the combination approached synergy with a ZIP score of 9.332. No synergy was found in other available prostate cancer cell lines with ZIP synergy score ranging from -3.201 to 3.637 (Supplementary Figure 3). Our data suggested that the combination of Ipatasertib and HRX-0233 effectively targets cell lines that are relatively resistant to Ipatasertib.

To gain more insight in the potential mechanism of synergy in PC3 cells, we aimed to delineate how mono- and combination therapy affect signaling cascades of mammalian target of rapamycin complex 1 (mTORC1), a major downstream target of activated AKT and MAPK [25]. Previous findings have suggested that mTORC1 and MAPK are interconnected on many levels and the cross-talks between these pathways are associated with resistance to PI3K inhibitors [9,11]. Additionally, inhibition of mTORc1 has shown to activate MAPK in PTEN-null prostate cancer in both *vitro* and *vivo* [26]. Hence, we conducted western blotting after 6h and 48h of mono- and combination treatment using phosphorylated ribosomal protein (p-S6) and phosphorylated eukaryotic initiation factor 4E-binding protein (p-4EBP1), as well as p90 ribosomal S6 kinase (p-RSK) and phosphorylated transcriptional factor Jun (c-Jun) as readouts for mTORC1 and MAPK signaling, respectively. We also included transcriptional factor Jun (c-Jun) which is a downstream target of MAP2K4 and cyclin D1 which is regulated by both mTORC1 and MAPK. Treatment with 2 μM Ipatasertib reduced level of p-S6, while combination of Ipatasertib and HRX-0233 reduced the levels of p-S6 and p-EBP1 even further at both 6h and 48h (Figure 2D). Focusing on the MAPK pathway, treatment with HRX-0233 alone showed a decrease p-RSK level at the 48h time point (Figure 2E). Mono-treatment with Ipatasertib showed an increase in p-RSK at 48h, in line with the previous findings that have shown that AKT inhibition increased level of p-ERK which is upstream of RSK [3]. Meanwhile, mono-treatment with HRX-0233 showed a decrease in p-RSK. Additionally, the combination demonstrated to decrease the level of both phosphorylated and c-Jun in comparison with the untreated and the mono treatments, especially at the 48h time point. Finally, mono-treatment with HRX-0233 was able to decrease the level of cyclin D1 at 6h timepoint, and the combination treatment led to an even stronger decrease in cyclin D1 level. Collectively, our results indicate that the synergy between Ipatasertib and HRX-0233 observed in PC3 cells could be mediated by synergistic effect on mTORC1 and MAPK signaling.

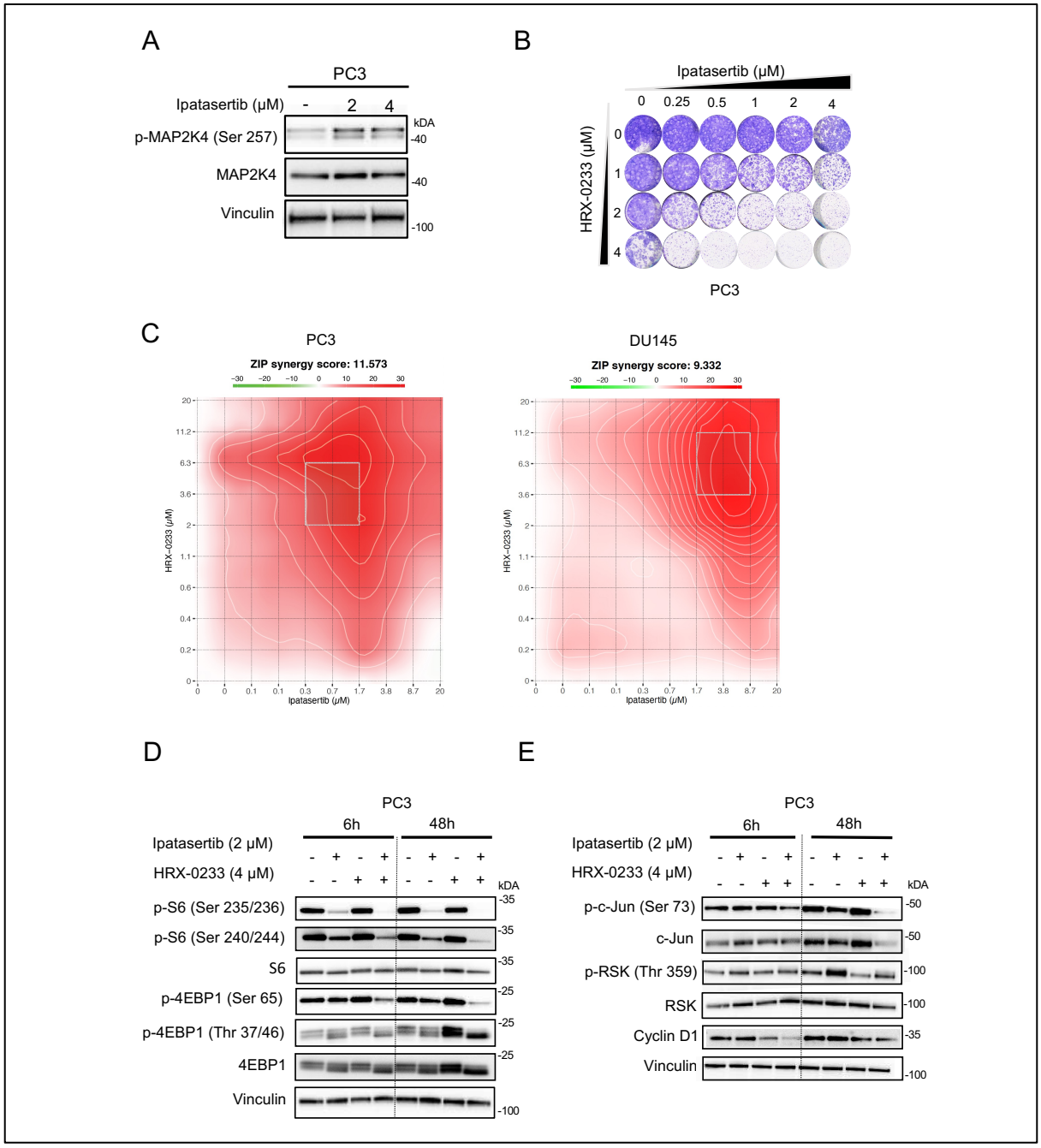

Figure 2: Synergy of Ipatasertib and HRX-0233. (A) PC3 cells were treated with 2 or 4 μM Ipatasertib for 6h, the levels of p-MAP2K4 and MAP2K4 were determined by western blot analysis. Vinculin served as loading control (A). (B) Colony formation assay of PC3 treated with indicated concentrations of Ipatasertib and HRX-0233 for 10 days. (C) Synergy distribution plots of PC3 and DU145 with ZIP synergy scores based on dose-response matrix of Ipatasertib and HRX-0233 combination. Red area indicates ranges of effective concentrations for synergy. ZIP score > 10 is considered synergy. (D) Effects of mono- and combination treatments with Ipatasertib and HRX-0233 on mTORC1 (E) and MAPK pathways. PC3 cells were treated with 2 μM Ipatasertib, 4 μM HRX-0233 or both. Cells were harvested at 6h and 48h. Vinculin served as loading control.

5.2 Genome-wide CRISPR knockout screen

To identify other targets for combination therapy, we performed a CRISPR knockout screen using a genome-wide human sgRNA library (Brunello) in PC3 cells treated with 2 μM Ipatasertib and 4 μM HRX-0233. (Figure 3A). CRISPR knockout screen is a powerful method to study to study the function of genes and their effects on the phenotype. The CRISPR knockout system makes use of Cas9 enzyme which is guided by a single guide RNA (sgRNA) to a specific genomic locus. Once arriving at the target, Cas9 induces a double-strand DNA break [47]. Cells repair the break by nonhomologous end joining (NHEJ), which is prone to error and causes insertions or deletions, which leads to frameshifts and/or a premature stop codon at the target gene that result in loss-of-function. During a genome-wide CRISPR screen, the sgRNAs targeting every gene in the genome are introduced into a cell population at low M.O.I to maximize the number of cells with only one sgRNA per cell. Consequently, each cell in the population experiences a single knockout event, but the targeted gene differ among cells. After subjecting the knockout cells to drug treatments of interest, the effect of a gene knockout can be quantified by comparing the relative depletions to the untreated population. Depleted sgRNAs would indicate candidate genes whose knockout can confer sensitivity to the treatment.

5.2.1 Screen optimizations for PC3

We generated PC3-Cas9 cells and quantified its expression using flowcytometry. We detected robust Cas9 expression in 82.5% of PC3 cells, resulting in effective gene editing in 85.5% of the cells (Figure 3B). To further optimize the screen condition we measured the cell doubling time of PC3-Cas9 by seeding cells at densities of 1, 1.5 and 2* 10^6 cells per 15 cm dish and counted the total cells after 5 days. We found that the average doubling time of PC3-Cas9 cells was 37h. The proper seeding density in a 15 cm dish was 1.5 million cells for appropriate confluency after 5 days (Figure 3C). To optimize drug concentration in the screen condition, we assessed toxicity of our compounds accounting for the seeding density of 1.5*10^6 cells per 15 cm dish. Ideally, we aimed for an IC30, as it would induce response without the drugs being overly toxic. We found that both 1 μM and 2 μM Ipatasertib corresponded with ±IC30 in PC3-Cas9 cell in 15 cm dishes. All included concentrations (2, 4 and 6 μM) of HRX-0233 showed growth inhibition above IC40 (Figure 3D). The drug concentrations corresponding to IC30 determined in this experiment were lower that the values from viability assay (~ 9 μM Ipatasertib and ~6 μM for HRX-0233), suggesting that the toxicity of the compounds depended on the culture condition. We also conducted Western blotting analysis to ensure that the Ipatasertib concentrations were effectively inhibiting the activity of AKT and MAP2K4 by measuring the relative amount of their downstream targets at 6h after treatment. It was evident that 1 μM Ipatasertib was already sufficient to lower the level of p-S6 at 6h, and that higher concentrations of Ipatasertib correlated with the decreased level of p-S6 (Figure 3E). HRX-0233 did not affect the level of MAP2K4 itself, its activation, nor of its downstream target C-Jun at 6h. Considering the data from drug synergy experiments in 5.1.2, we decided to proceed with 2 μM Ipatasertib and 4 μM HRX-0233 for the screen.

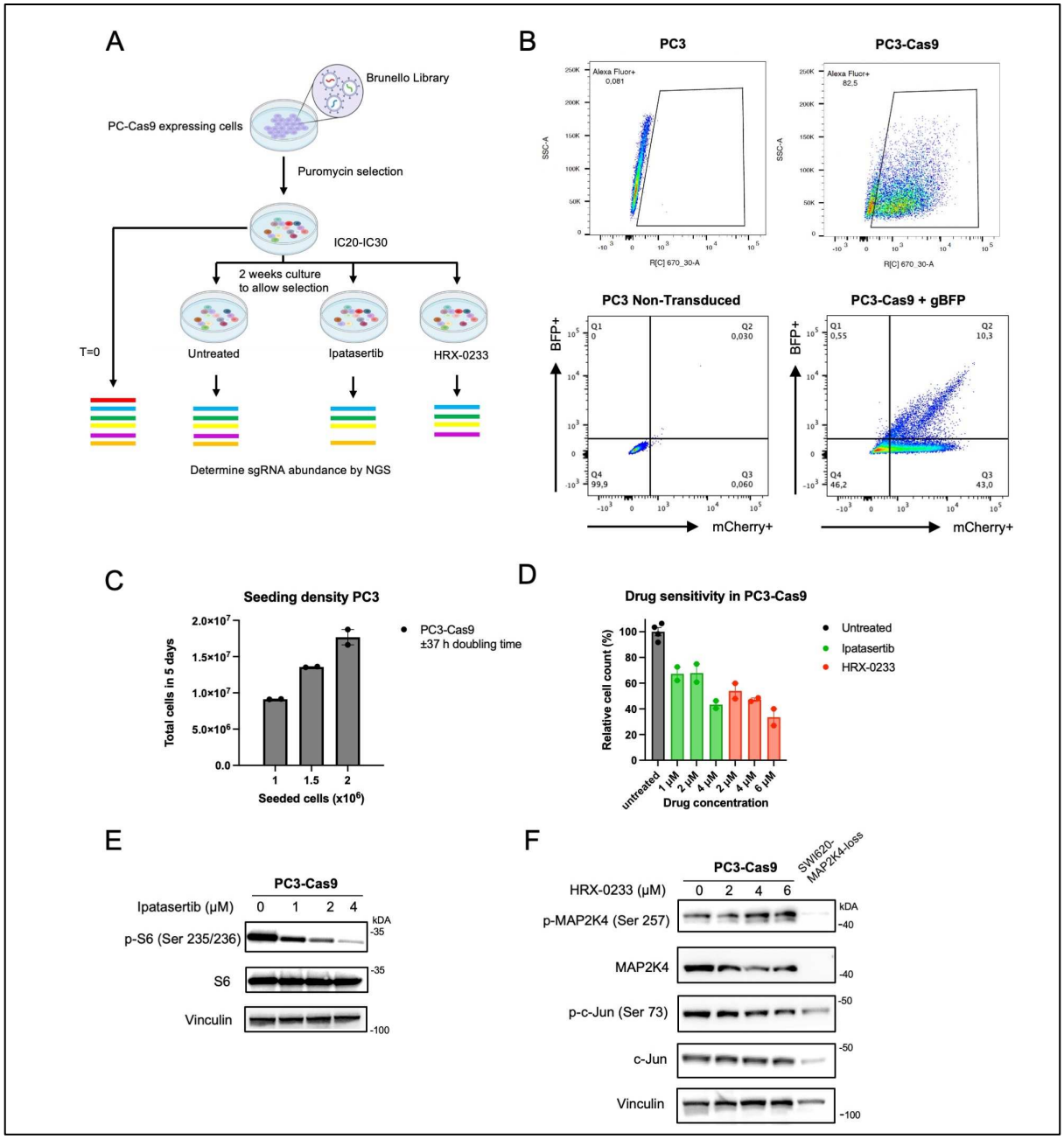

Figure 3: Genome-wide CRISPR-Knockout screen in PC3 cells. (A) Schematic outline of the CRISPR drop out screen used to identify gene knock out that increase sensitivity to Ipatasertib and HRX-0233. (B) Flowcytometry analysis of Cas9 expression and Cas9 editing efficiency in PC3. Cas9 expressing cells are positive for Alexa Fluor. PC3-Cas9 cells were infected with lentivirus containing BFP, mCherry and sgRNA targeting BFP. Cells with successful gene editing showed low BFP fluorescent signals and high mCherry signals as represented in Q3. (C) PC3-Cas9 seeded at different densities in 15 cm dish. The total amount of cells was counted after 5 days and the average doubling time was calculated. (D) Cell counts of PC3-Cas9 treated with 1, 2 or 4 µM Ipatasertib (green) and cell cell count of PC3-Cas9 treated with 2, 4 or 6 µM HRX-0233 (red) relative to the untreated population (black). (E) S6 and p-S6 levels in PC3-Cas9 treated with 0, 1, 2 or 4 µM Ipatasertib for 6h (F) p-MAP2K4, MAP2K4, p-c-Jun and c-Jun levels in PC3-Cas9 treated with 0, 2, 4 or 6 µM HRX-0233. Lysate of SWI620$^{(PTEN-/-)}$ served as a positive control. Vinculin served as a loading control.

5.2.2 Drop out screen identifies Cyclin D1 as a vulnerable target to Ipatasertib treatment in PC3

PC3-Cas9 cells containing sgRNA were cultured for 14 days with or without 2 μM Ipatasertib or 4 μM HRX-0233, using 3 biological replicate cultures. We found that 2 μM Ipatasertib treated population was ~40% of the untreated population, indicating that the compound was more toxic (IC60) than previously determined during the screen optimizations (IC30). 4 μM HRX-0233 treated population was ~38% of the untreated population (IC62), also showing more toxicity relatively to the prior result (IC50) (Figure 4A). All cells were passaged 3 times before the complex pool of gene edited cells in the different conditions was harvested. To determine whether the treatment induced selection or depletion of specific sgRNAs, we performed NGS and the abundance of sgRNAs analyzed with drugZ [48]. The abundance of sgRNAs in 3 replicates of each condition showed high correlation (R^2 = 0.852-0.918), indicating robust and reproducible findings (Supplementary Figure 4). To determine the efficacy of gene editing, we analyzed a pool of sgRNAs targeting lethal genes, which showed median gene depletion of log2FC of -1.5 in the treated vs. untreated condition. The negative control consisted of sgRNAs targeting non-essential genes showed no statistically significant difference of depleted sgRNAs (Supplementary Figure 3). We used a standard cut off of FDR <= 0.25 to assess statistical significance of depleted sgRNAs. We generated negative selection of genes that increases sensitivity of cells to the treatments. Negative selections with Ipatasertib identified 4 hits that were depleted: *CCND1*, *NUDT10*, *NUP93* and *WDR24* (Figure 4B). Here, we found that sgRNAs targeting *CCND1* (gene encoding cyclin D1) were most depleted in the Ipatasertib treated condition compared to the untreated condition (log2FC = -1.02, FDR = 0.0078), followed by *NUP93* (log2FC = -0.39, FDR = $7.39*10^{-8}$), *WDR24* (log2FC = -0.41, FDR = 0.06) and *NUDT10* (log2FC = -0.39, FDR = $7.39*10^{-8}$). On the other hand, negative selections with HRX-0233 identified 9 hits in total; *SPPL3* (log2FC = -1.0, FDR = $1.69*10^{-5}$), *VAC14* (log2FC = -0.93, FDR = $7.64*10^{-11}$), *FIG4* (log2FC = -0.80, FDR = $1.19*10^{-7}$), *PPP1CA* (log2FC = -0.78, FDR = $4.13*10^{-5}$), *IRF2BPL* (log2FC = 0.65, FDR = 0.018), *PPP4R2* (log2FC = -0.56, FDR = 0.0189), *BACH1* (log2FC = -0.58, FDR = 0.0189), *TRIB3* (log2FC = -0.49, FDR = 0.097) and *RNF25* (log2FC = -0.43, FDR = 0.197) (Figure 4C). Protein-protein interaction analysis revealed that VAC14 and FIG4 form a complex, and that PPP1CA and PPP4R2 are both related to each other (Supplementary figure 6B). The positive selections of the drop out screens are presented in the Supplementary Figure 4 & 5. Overall, our screen data showed that the depletion of cyclin D1 had the most impact on cell survivability specifically during Ipatasertib treatment.

To validate the effect of cyclin D1 depletion, we investigated the combination of Ipatasertib and CDK4/6 inhibitor Palbociclib in PC3 cells, as cyclin D1 needs to form a complex with CDK4/6 to activate downstream targets [27]. Palbociclib exhibited IC50 = 7.7 μM in PC3 cells. A short-term viability assay was conducted and the synergy score was calculated in the same manner as described in 3.1.2. The ZIP synergy score for this combination was 4.623, which was lower than the standard indication for a significant synergy (Figure 4D). Consistently, long-term colony formation assay showed that the combination of Ipatasertib and Palbociclib impaired cell proliferation to some degree (Figure 4E). These results confirm that Palbociclib sensitizes PC3 cells to Ipatasertib. We did not observe synergy between these two compounds.

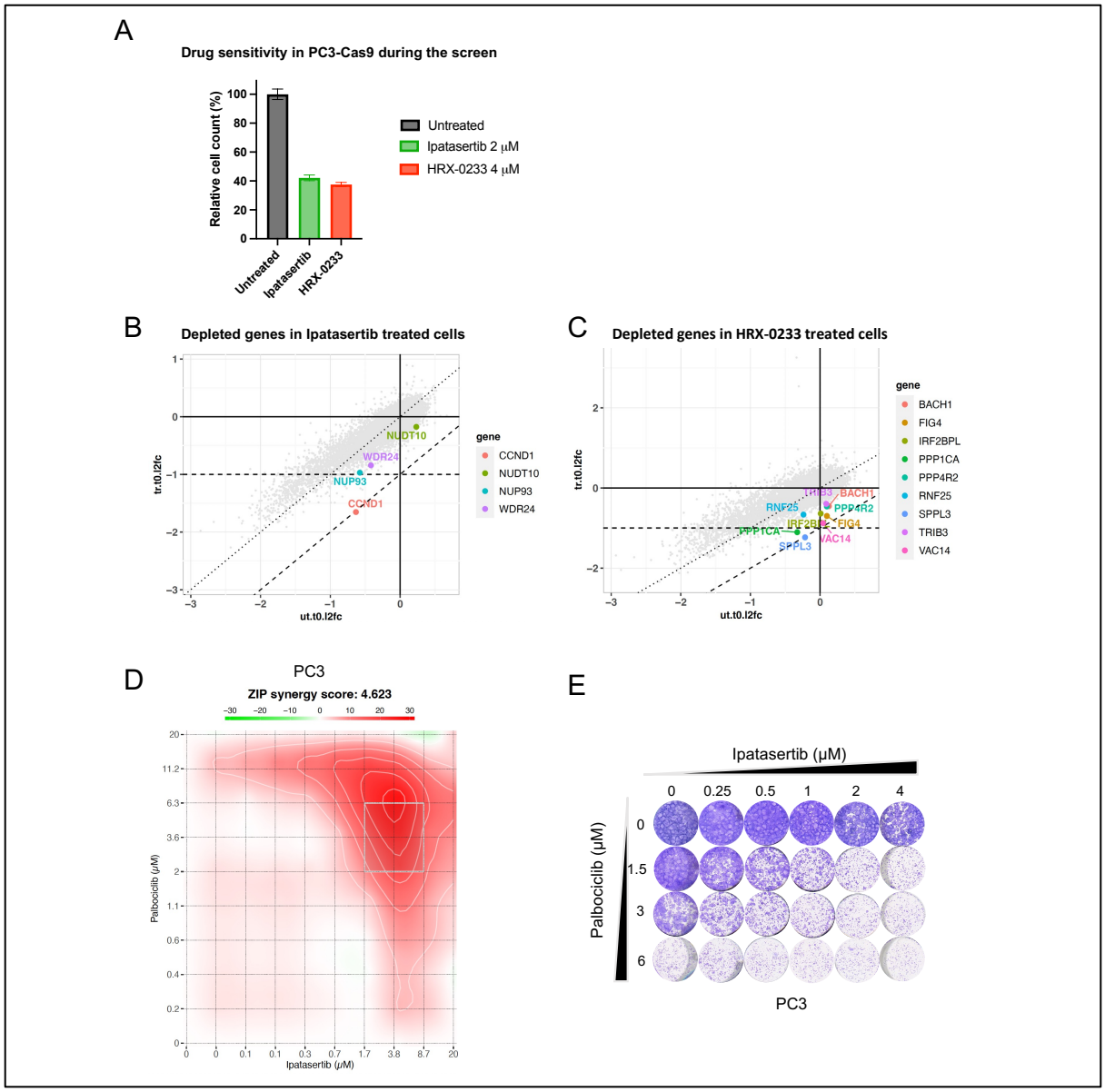

Figure 4: Identification and validation of cyclin D1 as Ipatasertib sensitizer. (A) Amount of PC3-Cas9 cells treated with 2 µM Ipatasertib (green) or 4 µM HRX-0233 (red) relative to untreated population (black). (B) Volcano plots identified depleted genes of the screen with Ipatasertib, and with (C) HRX-0233. X-axis represents log2FC in the untreated condition vs. untreated condition at time point 0 (T=0). Y-Axis represents log2FC in treated condition vs. untreated condition. Log2FC < -1 in treated vs. untreated condition is considered a significant impact. (D) Synergy distribution plot of PC3 ZIP synergy scores based on dose-response matrix of Ipatasertib and Palbociclib combination. Red area indicates ranges of effective concentrations for synergy. ZIP score > 10 is considered synergy (E) Colony formation assay of PC3 treated with indicated concentrations of Ipatasertib and Palbociclib for 10 days

5.3 Overactivation of oncogenic signaling in PTEN-loss CRPC

We hypothesize that AR and/or AKT could be therapeutic targets in mCRPC based on the principle of overactivation of oncogenic signaling. We performed a drop out screen using the PP2A in inhibitor LB-100 (1 μM) and supraphysiological concentrations of synthetic androgen R1881 (5 nM) (Figure 5A). We used LnCap-abl as a model for PTEN-null, AR positive and castration resistant prostate cancer characteristics as shown in 5.1.1.

5.3.1 Screen optimizations for LnCap-abl

Similarly to the previous screen we conducted, LnCap-abl cell line expressing Cas9 was generated. The expression and the editing efficiency of Cas9 were quantified by flow cytometry. We detected substantial expression of Cas9 in 90.8 % and a successful gene editing in 50% in LnCap-abl cells. (Figure 5B). Given the low editing efficiency, the LnCap-abl-Cas9 were infected with 1 system lentivirus containing both sgRNA library and sequence encoding for Cas9 to increase the editing probability. We determined cell doubling time by seeding cells at densities of 1.5, 2 and 3*10 cells per 15 cm dish and counted the total cells after 7 days. The average doubling time was 48h and $2*10^6$ cells were appropriate seeding density in 15 cm dish after 7 days (Figure 5C). We also assessed toxicity as well as potential drug build-up effect of our compounds accounting for the chosen seeding density by culturing cells in the presence of 1, 1.5 or μM LB-100, or in 2.5, 5 or 10 μM R1881. We found that 1 μM LB-100 μM initially had no significant effect on cell proliferation after 7 days, but an ±IC40 was observed after reseeding and drug refreshment (Figure 3D). All of the included concentrations of R1881 (2.5, 5 and 10 nM) in treated condition showed minor difference in cell proliferation after 7 days, ranging from IC40 to IC60 (Figure 3E). Additionally, we conducted Western blotting analysis to ensure that the LB100 concentrations were effectively inhibiting the activity of PP2A using p-AKT (Thr 308) and p-c-Jun as readouts, and that R1881 concentrations were affecting AR signaling using PSA as readouts at 8h after treatment. It was evident that 1 μM LB-100 was already sufficient to increase the level of p-AKT (Thr 308) in particular and p-c-Jun within 8h. (Figure 3E). All R1881 concentrations that were included led to an increased level of PSA to a similar level. The level of PSA was indeed increased in the R1881 treated population. Therefore, 1 μM LB-100 and 5 nM R1881 were chosen for the screen that correspond to IC20-30.

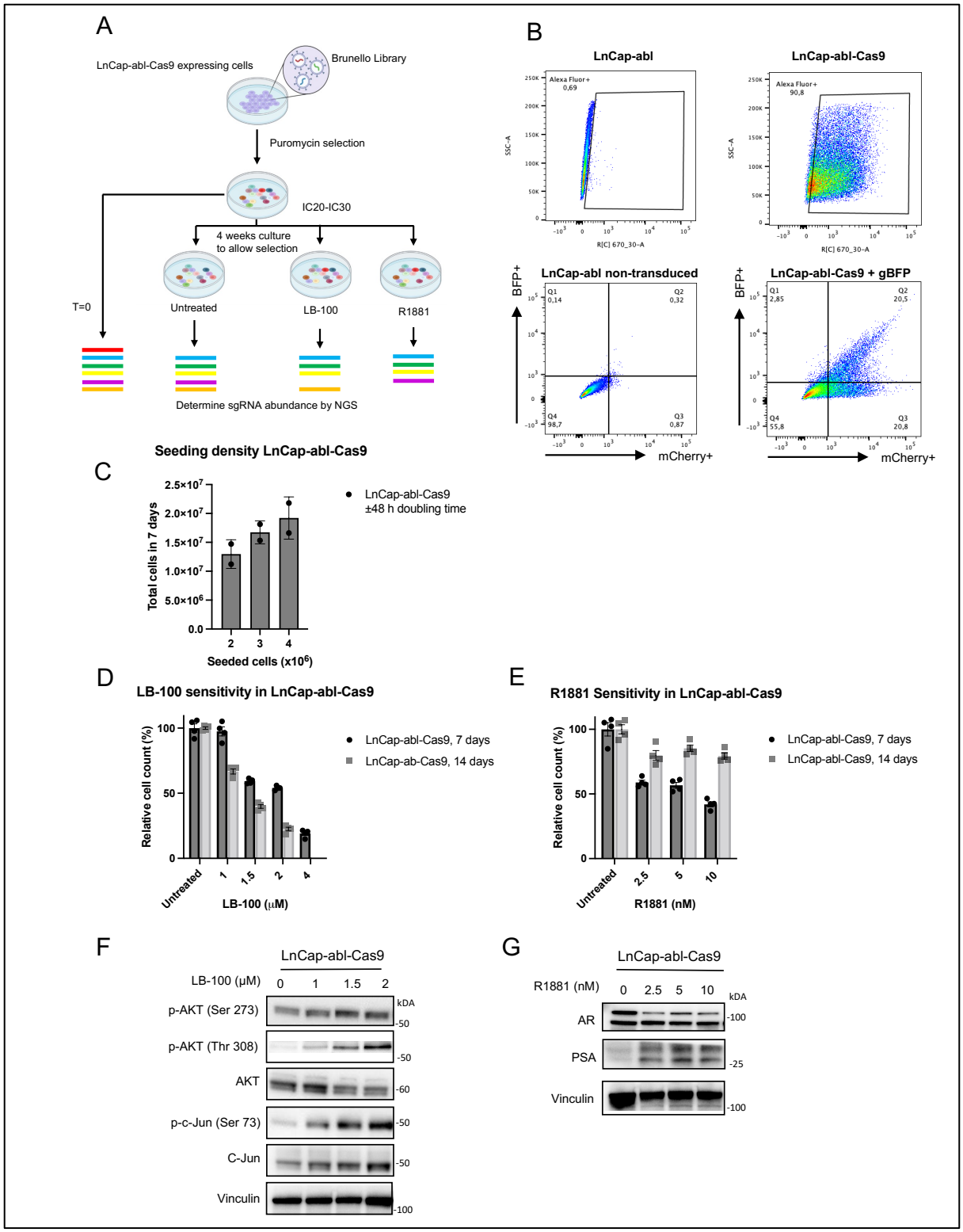

Figure 5: Genome-wide CRISPR-Knockout screen in LnCap-abl cells. (A) Schematic outline of the CRISPR drop out screen used to identify gene knock out that increase sensitivity to LB-100 and R1881. (B) FACS analysis of Cas9 expression and Cas9 editing efficiency in LnCap. Cas9 expressing cells are positive for Alexa Fluor. LnCap-abl-Cas9. Cells with successful gene editing showed low BFP fluorescent signals and high mCherry signals as represented in Q3. (C) LnCap-abl-Cas9 seeded at different densities in 15 cm dish. The total amount of cells was counted after 7 days and the average doubling time was calculated. (D) Cell counts of LnCap-abl-Cas9 treated with 1, 1.5 or 2 µM LB-100 relative to the untreated population after 7 days (black) and after 14 days with 1 passage (gray) (E) Cell count of LnCap-abl-Cas9 treated with 2.5, 5 or 10 nM relative to the untreated population after 7 days (black) and after 14 days with 1 passage (gray) (F) p-AKT, AKT, p-cJun and c-Jun levels in Lncap-abl-Cas9 treated with 0, 1, 1.5 or 2 µM LB-100 for 8h. (F) AR and PSA levels in LnCap-abl-Cas9 treated with 0, 2.5, 5 or 10 nM R1881. Vinculin served as a loading control.

5.3.2 Genome-wide CRISPR knockout screen in LnCap-abl identified multiple candidate genes as vulnerable targets for overactivation of PI3K/AKT and AR signaling in Lncap-abl cells.

We performed a genome-wide CRISPR screen in a PTEN-loss, castration resistant LnCap-abl cell line. After integration of sgRNAs and proper cell attachment, cells were treated with or without 1 μM LB-100 or 5 nM. We found 1 μM LB-100 treated population was ~50% of the untreated population, indicating more toxicity (IC50) than previously determined during the screen optimizations. Similarly, 5 nM R1881 treated population was ~37% of the untreated population (IC63), also showing more toxicity (Figure 4A). Following 4 cells passages, the pool of gene edited cells of each condition was collected. We quantified the abundance of sgRNA by NGS. The abundance of sgRNA in 3 replicates showed lower correlation than ideal (R^2= 0.335-0.919). To determine the efficacy of gene editing, we analyzed the pool of sgRNAs targeting lethal genes, which showed median gene depletion of log2FC of -1.5 in the treated vs. untreated condition. The negative control consisted of sgRNAs targeting non-essential genes showed no difference in log2FC (Supplementary Figure 5). Sensitizer genes were identified as gRNAs significantly depleted (FDR <= 0.25) in LB-100 and R1881 treated cells compared to the untreated cells using drugZ [48] . DrugZ data of the screen with LB-100 revealed 22 depleted genes in total. To ensure that these hits are robust, we selected the top 5 hits with the largest log2FC in the treated vs untreated population, whilst showing minimal effect in the untreated vs T_0 population. These top 5 hits being: *CDH1* (log2FC = -2.191, FDR = $-4.8*10^4$), *KIF18A* (log2FC = -1.94, FDR = 0.18) *, KPNA6* (log2FC = -1.94, FDR = $-3.4*10^4$)*, DYNC1I2* (log2FC = -1.94, FDR = $-3.48*10^3$) and *ITFG3* (log2FC = -1.73, FDR = $-1.43*10^4$). Protein-protein analysis showed that *CDH1*, *ALCAM* and *FYN* are candidate genes that are related to each other (Supplementary figure 7). In parallel, the screen with R1881 identified 4 hits that were depleted: *AXIN1* (log2FC = -2.43, FDR = $-7*10^5$)*, STK35* (log2FC = -1.83, FDR = -0.019)*, MECOM* (log2FC = -2.1, FDR = -0.03) and *C1orf127* (log2FC = -1.61, FDR = -0.23). The positive selections of the knockout screens are presented in the Supplementary Figure 8 & 9.

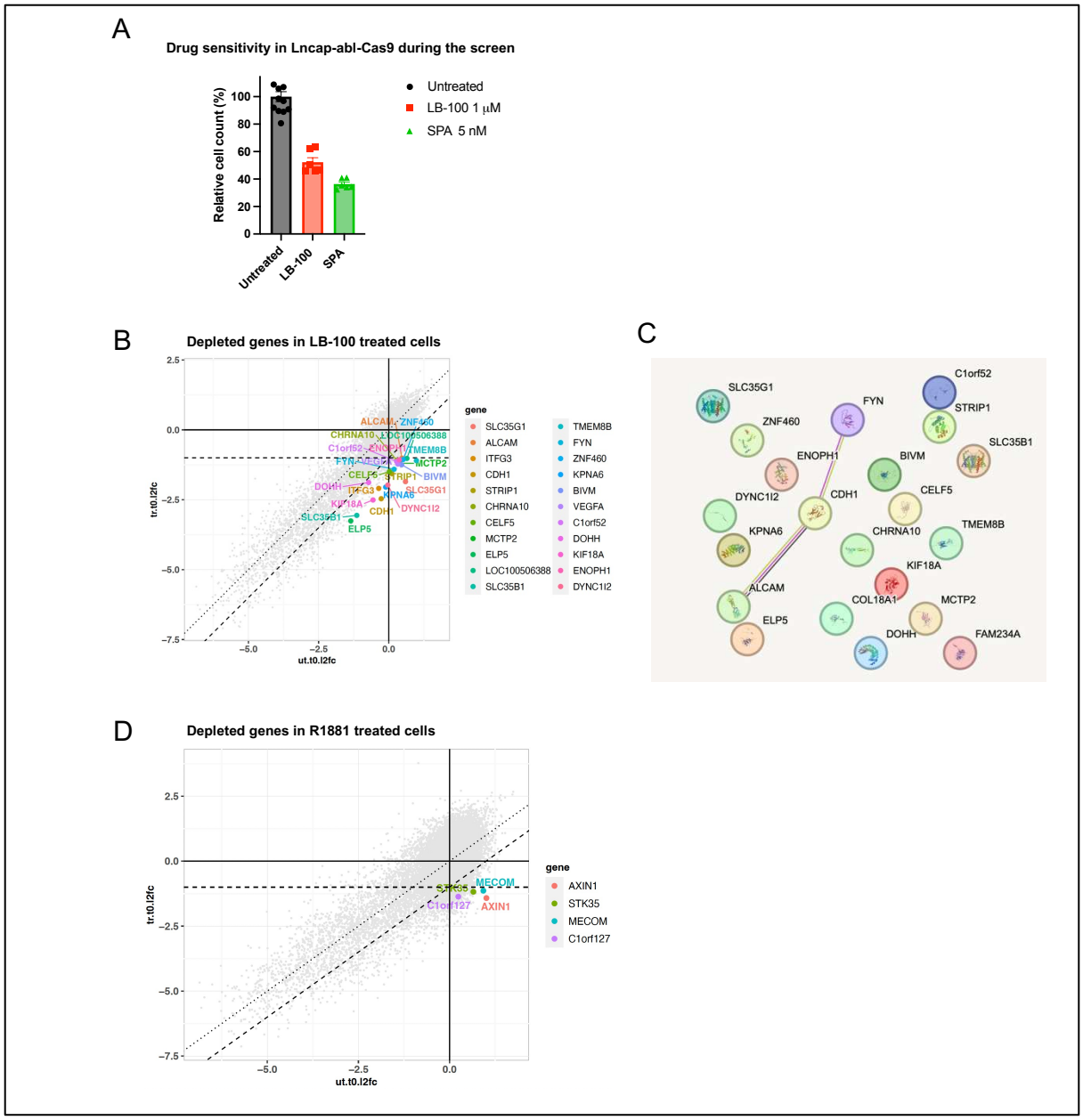

Figure 6: Identification LB-100 and R1881 sensitizers. (A) Amount of LnCap-abl cells treated with 1 μM LB-100 (green) or 5 nm R1881 (red) relative to untreated population (black). (B) Volcano plots identified depleted genes of the screen with LB-100, and with (D) R1881. X-axis represents log2FC in the untreated condition vs. untreated condition at time point 0 (T=0). Y-Axis represents log2FC in treated condition vs. untreated condition. Log2FC < -1 in treated vs. untreated condition is considered a significant impact. (C) STRING pathway analysis showing protein-protein association between ALCAM, CDH1 and FYN.

6. Discussion

Metastatic castration resistant prostate cancer is a lethal disease with no effective cure. This advanced stage of prostate cancer no longer responds to the conventional androgen deprivation therapy that involves AR signaling blockade. The loss of functional PTEN tumor suppressor is present in up to 50% of metastatic prostate cancer patients contributes to the AR independent state as well as a hyperactivation of the AKT pathway. Inhibiting AKT showed limited clinical benefit due to acquired resistance and complex cross-talks with other signaling pathways, which can counteract the inhibitory effects of drugs. Our initial results demonstrated wide discrepancy in response to AKT inhibitor Ipatasertib between different prostate cancer cell lines, reflecting the diverse clinical response in mCPRC patients. Many efforts have been made to develop combination therapy based on AKT inhibition to improve clinical outcome in resistant sup group of patients [6,7,8,40]. However, current combinations have shown to be marginally beneficial, discovery of new combination therapy deems urgent to overcome resistance and maximize efficacy of Ipatasertib.

The first part of our study evaluated the efficacy of Ipatasertib treatment in combination with HRX-0233, based on the increased activity of MAP2K4 observed in Ipatasertib treated cells. The same observation was found in breast cancer [11]. The elevated activation of MAP2K4 is induced as rapid as within 6 hours, suggesting that this process occurs via signaling interaction rather than via transcriptional activity or genetic changes. Ipatasertib treatment in combination with HRX-0233 has never been investigated before. Here, we found that Ipatasertib and HRX-0233 synergize in PTEN-deficient and AR independent cell line PC3 and strong enhancing effects in the DU145 PTEN-expressing cell line. The lack of synergy in other PTEN-deficient cell lines suggests that the synergy does not occur due to general dependency and more likely due to cell line-related factors. Also, other cell lines already showed high sensitivity to Ipatasertib that decreased the window of synergy with HRX-0233. Based on our observations, it is possible that the Ipatasertib and HRX-0233 combination would yield greater benefit in AR negative prostate cancer, which is a common aspect of these two cell lines. Previous studies have focused on other Ipatasertib-based combination possibilities, such as with PIM inhibitor and Bcl-2 inhibitor Navitoclax [28, 29], but no synergy was observed in AR-negative prostate cancer. Our findings may therefore provide novel combination therapy for AR-negative mCPRC patients. Regarding the potential mechanisms, we observed that the combination managed to further downregulate mTORC1 and MAPK pathways, specifically p-S6, c-Jun and cyclin D1 with respect to the use of single inhibitor. Similar observations can be found in the study of breast cancer, which showed decreased level of p-S6 upon PI3K inhibition in MAP2K4 knockdown cell lines [11]. It is well established that pathway reactivation via mTORC1 is often found upon AKT inhibition in cancer with PTEN loss mutation, as well as upregulation of MAPK signaling via cross-talks. Furthermore, c-Jun is required for the transcription of cyclin D1 [33]. Our results suggest that synergy of Ipatasertib and HRX-0233 is likely achieved due to impaired activation of mTORC1 and prevented cross-talks with MAPK, both resulted in cyclin D1 depletion. Still, future experiment is necessary to elucidate the molecular interactions and mechanism of death. Future experiments could utilize phosphoproteomics to define signaling networks regulation and dysregulation. We could also further investigate whether cell death caused by Ipatasertib and HRX-0233 combination is mediated by autophagy or by apoptosis, since mTORC1 is known to be an important negative regulator of autophagy. Of note, we were unable to verify specificity of HRX-0233 to MAP2K4 and cannot rule out the possibility that the other off-targets or the downstream targets of MAP2K4 such as p38, JNK or c-Jun are mainly responsible for the synergy. As shown in our experiment, treatment with HRX-0233 alone did not affect the levels of p-c-Jun. We could examine the effect of HRX-0233 on MAP2K4 activity, as well as to test the effect of Ipatasertib in cells with low levels of MAP2K4, p38, JNK or c-Jun, using knock down cells or inhibiting compounds for example.

The second part of our study made use of genome-wide CRISPR screen to unbiasedly identify genetic dependencies that may be explored as potential therapeutic targets. Our screen results showed that *CCND1* was depleted with the largest effect size in Ipatasertib treatment, demonstrating that cyclin D1

loss caused cells to be relatively vulnerable to Ipatasertib. cyclin D1 is a key regulator of the G_1 phase of the cell cycle, and its overexpression is associated with metastatic prostate cancer to the bone [35]. To further validate the effect of cyclin D1 inhibition, Palbociclib was used in combination with Ipatasertib in PC3 cells. Although our findings showed that that the combination was not synergistic but rather additive based on cell viability assay, strong inhibitory effect on long-term cell proliferation was observed, suggesting that Palbociclib is able to sensitize PC3 cells to Ipatasertib. In fact, multiple studies and an ongoing clinical trial in HER2-negative breast cancer have provided evidence that dual inhibition cdk4/6 inhibitor and AKT inhibitor is more effective than single drug treatments [30, 31]. Importantly, study in mCRPC-patient derived xenograft revealed 75% decrease in tumor size in the Palbociclib-Ipatasertib treated group and the in vivo experiment is in progress [32]. Interestingly, combination treatment of Palbociclib and Ipatasertib was less synergistic comparing to combination with Ipatasertib and HRX-0233 that we have recently evaluated. Akin to cyclin D1 inhibition by Palbociclib, the combination treatment with Ipatasertib and HRX-0233 also showed diminishing levels of cyclin D1. Our collective results therefore support the possibility that synergy of Ipatasertib and HRX-0233 is partly due to the depletion of cyclin D1, and the superior efficacy of Ipatasertib-HRX-0233 combination is supposedly due to dual mTORC1 and MAPK inhibition upstream of cyclin D1. Unlike Palbociclib-Ipatasertib combination, the novel synthetic lethal combination of Ipatasertib-HRX-0233 still needs validation in vivo models as well as assessment of overlapping toxicity to assist design of translation to the clinic.

Our screen result also showed that VAC14 and FIG4 are depleted in HRX-0233 treatment. Both genes encode for proteins belong to the same complex PIKfyve-Vac14-Fig4, facilitating conversion between phosphatidylinositol-3-phosphate (PtdIns3P) and phosphatidylinositol-3,5-bisphosphate ($PtdIns(3,5)P_2$). Previous study in cellular interactome of VAC14 and FIG4 revealed that both proteins can physically interact with proteins in PI3K/AKT pathway [36]. Moreover, targeting PIKfyve pathway which results in the inhibition of autophagy can sensitize prostate cancer cells to immunotherapy [35], suggesting a potential combination use of HRX-0233 and PIKfyve/autophagy inhibitors such as ESK981.

The third part of our study exploited the high oncogenic signaling in PTEN-null castration resistant prostate cancer cells, particularly by overactivation of AKT pathway and AR signaling using LB-100 and R1881. We identified multiple candidate genes whose knockout sensitize LnCap-abl cells to LB-100 and R1881 utilizing genome-wide CRISPR screen. Among our selected top 5 hits, *CDH1, KIF18A and DYNC1I2* encode structural proteins critical for the formation of mitotic spindle and their depletion would result in improper chromosome segregation during mitosis [41, 42, 43, 44, 45]. Our screen data therefore suggest a possibility that overactivation of oncogenic signaling by LB-100 intensifies the dependence on mitotic stress and that in combination with the depletion of *CDH1, KIF18A and DYNC1I2* would induce mitotic catastrophe. Furthermore, we performed a screen with R1881 to discover genes whose knockout is selectively toxic in the presence of the drug. We found that LnCap-abl-Cas9 became less sensitive to R1881 after 14 days of consecutive culturing under drug pressure, lowering the inhibitory effect to ±IC20-30. This suggests that these cells rapidly adapt to the supraphysiological levels of androgen and prolonged treatments with R1881 would not be effective. Our screen data revealed AXIN1 among other candidate genes whose depletions enhance the efficacy of R1881. *AXIN1* encodes for AXIN, which is a pivotal component of the β-catenin destruction complex [45]. Depletion of AXIN would disrupt this complex, leading to β-catenin accumulation in the cytoplasm that can translocate to the nucleus and ultimately activate Wnt pathway [46]. Additionally, β-catenin is a coactivator of the AR and stimulates AR transcriptional activity. Our data indicates that the overload of AR signaling is lethal in PTEN-null castration resistant prostate cancer. However, further validation experiments are necessary to confirm our findings.

In conclusion, our study underlines the potential for novel combination treatments with Ipatasertib and HRX-0233 in AR-negative prostate cancer. We also provide vulnerable targets to the overactivation of

oncogenic signaling that should be considered when exploring alternative therapeutic strategy for PTEN-null castration resistant prostate cancer.

7. Supplementary

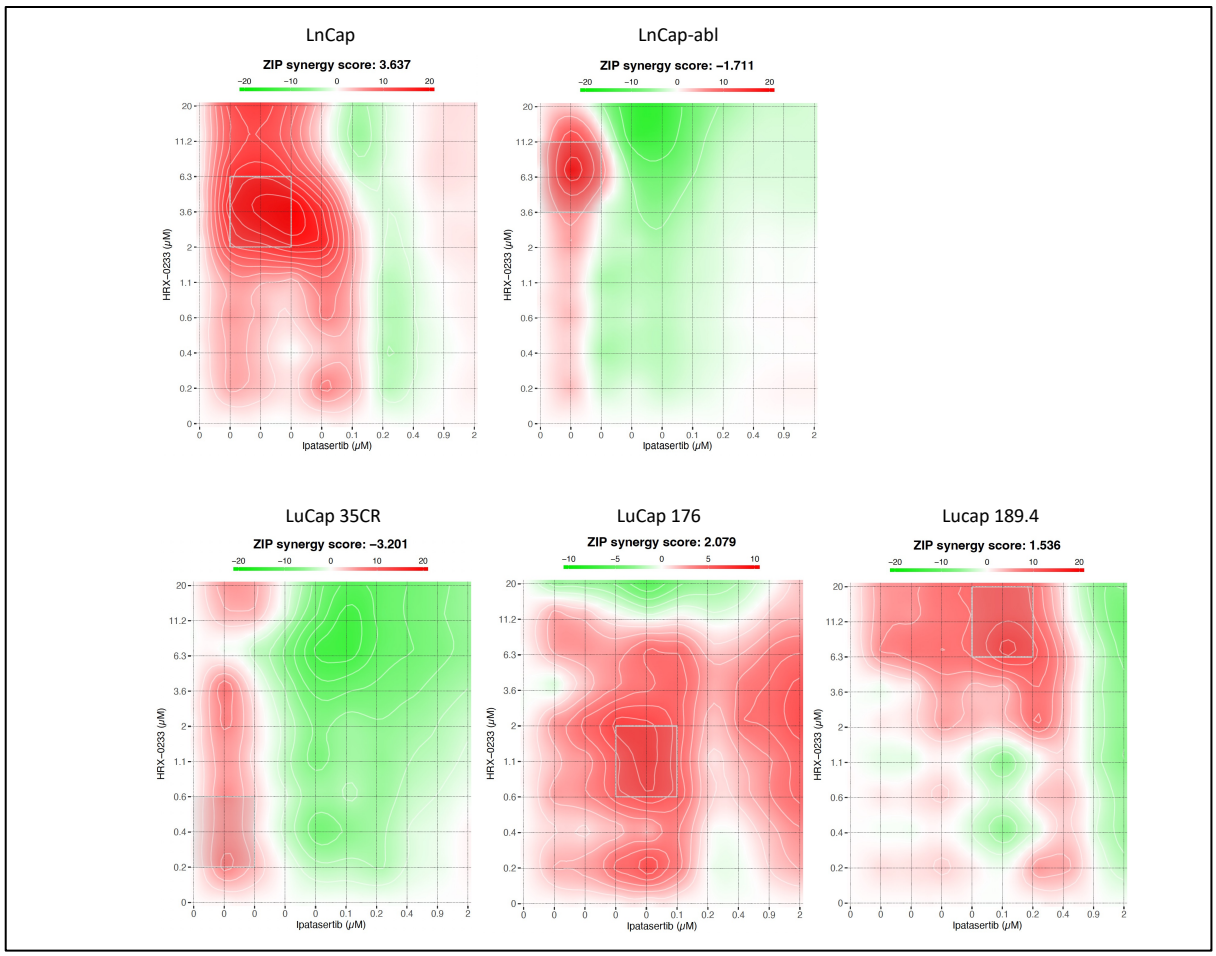

Supplementary figure 1: Ipatasertib and HRX-0233 combination is not synergistic in PTEN-loss Ipatasertib resistant cell lines. Synergy distribution plots of LnCap, LnCap-abl, Lucap 35CR, LuCap 176 and LuCap 189.4 with ZIP synergy scores based on dose-response matrix of Ipatasertib and HRX-0233 combination. Red area indicates ranges of effective concentrations for synergy. ZIP score > 10 is considered synergy**.**

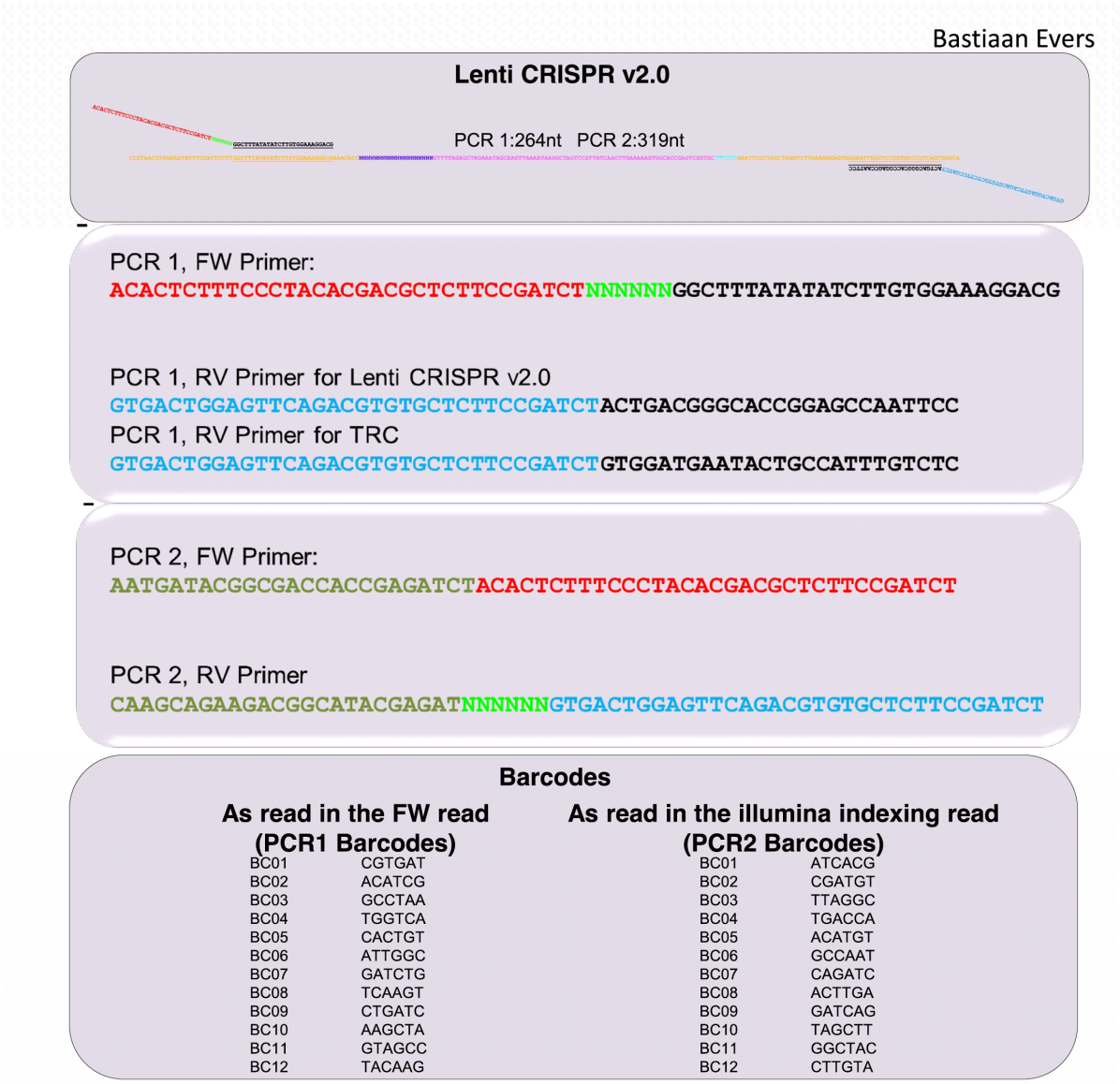

Supplementary Figure 2: Primers design for PCR1 and PCR2 to prepare samples for NSG (adapted from DNA capture protocol for Lentiguide-based library and for LentiCRISPR2.1-based library screens. PCR1 incorporates an Illumina sequencing primer sequence (red) and a barcode (green) into the forward read. The barcode enables independent indexing of each condition during the screen and facilitates the analysis of the combined sequencing results. PCR2 introduces the necessary P5 and P7 adapters (dark green) to attach to the Illumina flow cell, along with an extra barcode sequence. This additional barcode can be read through when an Illumina indexing read is requested from the Genomics Facility.

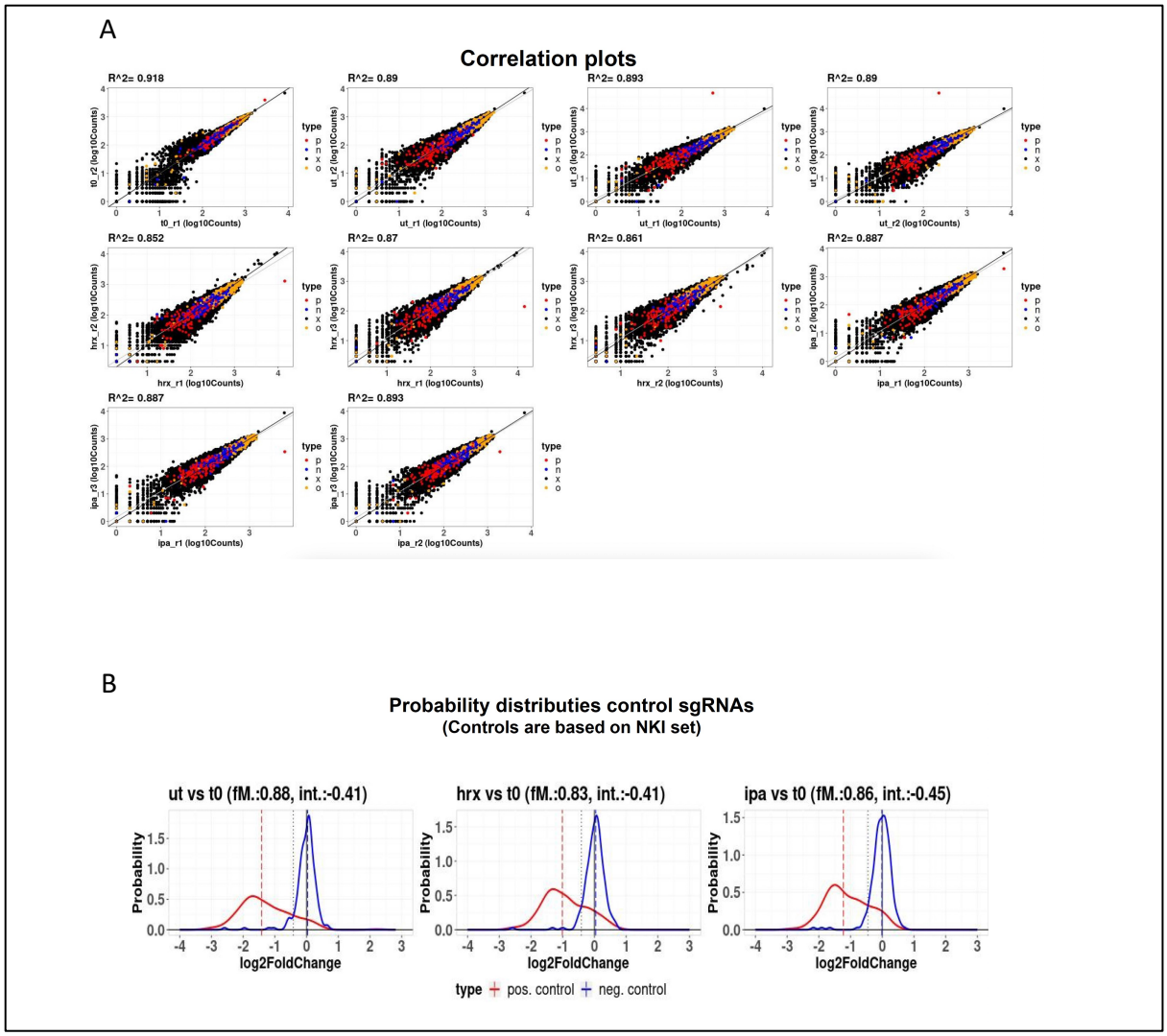

Supplementary figure 3: Quality control of genome-wide CRISPR screen in PC3 cells. (A) Correlation plots of all sgRNA reads between each replicate. (B) Probability distribution of control sgRNAs of each screen condition vs untreated condition at T=0.

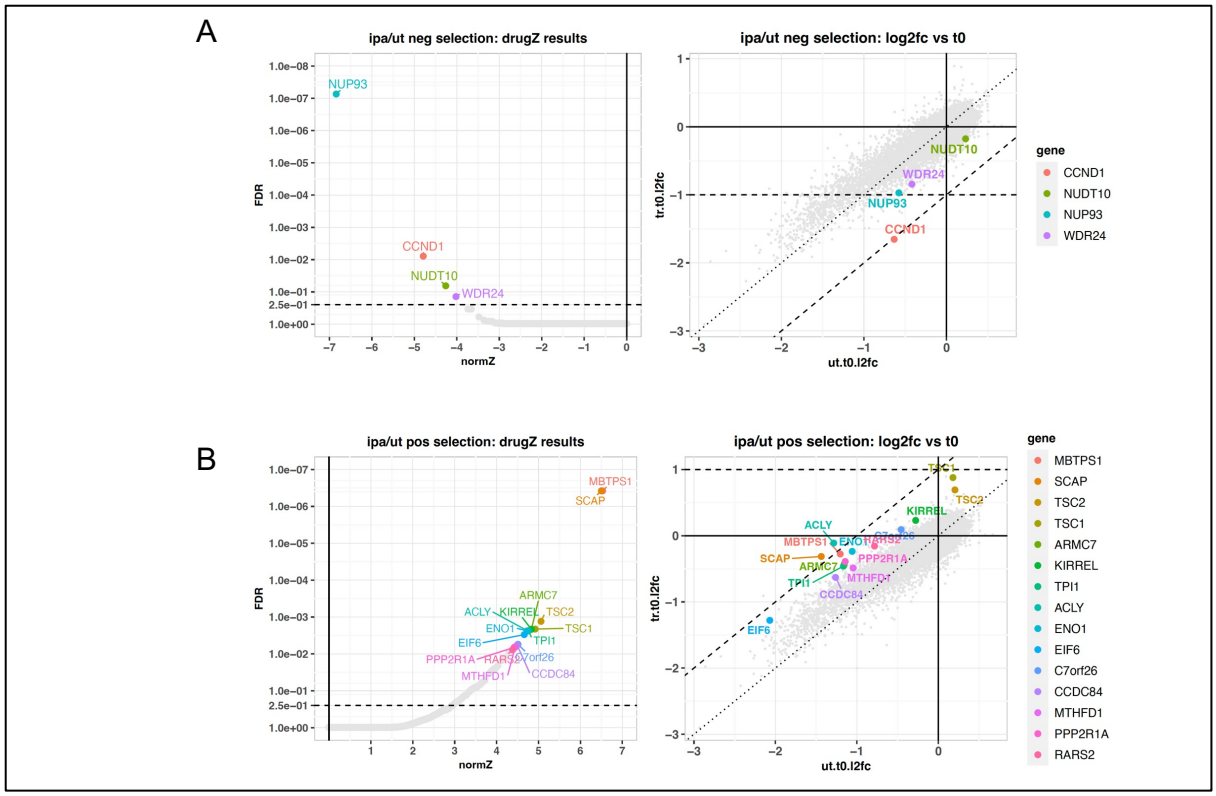

Supplementary figure 4: Genome-wide CRISPR knockout screen in PC3 with Ipatasertib. (Left panel) False discovery rate (FDR) of top ranked depleted sgRNAs (A), and of top ranked enriched sgRNAs (B). (Right panel) Volcano plots identified depleted genes of the screen with Ipatasertib. X-axis represents log2FC in the untreated condition vs. untreated condition at time point 0 (T=0). Y-Axis represents log2FC in treated condition vs. untreated condition. Log2FC < -1 in treated vs. untreated condition is considered a significant.

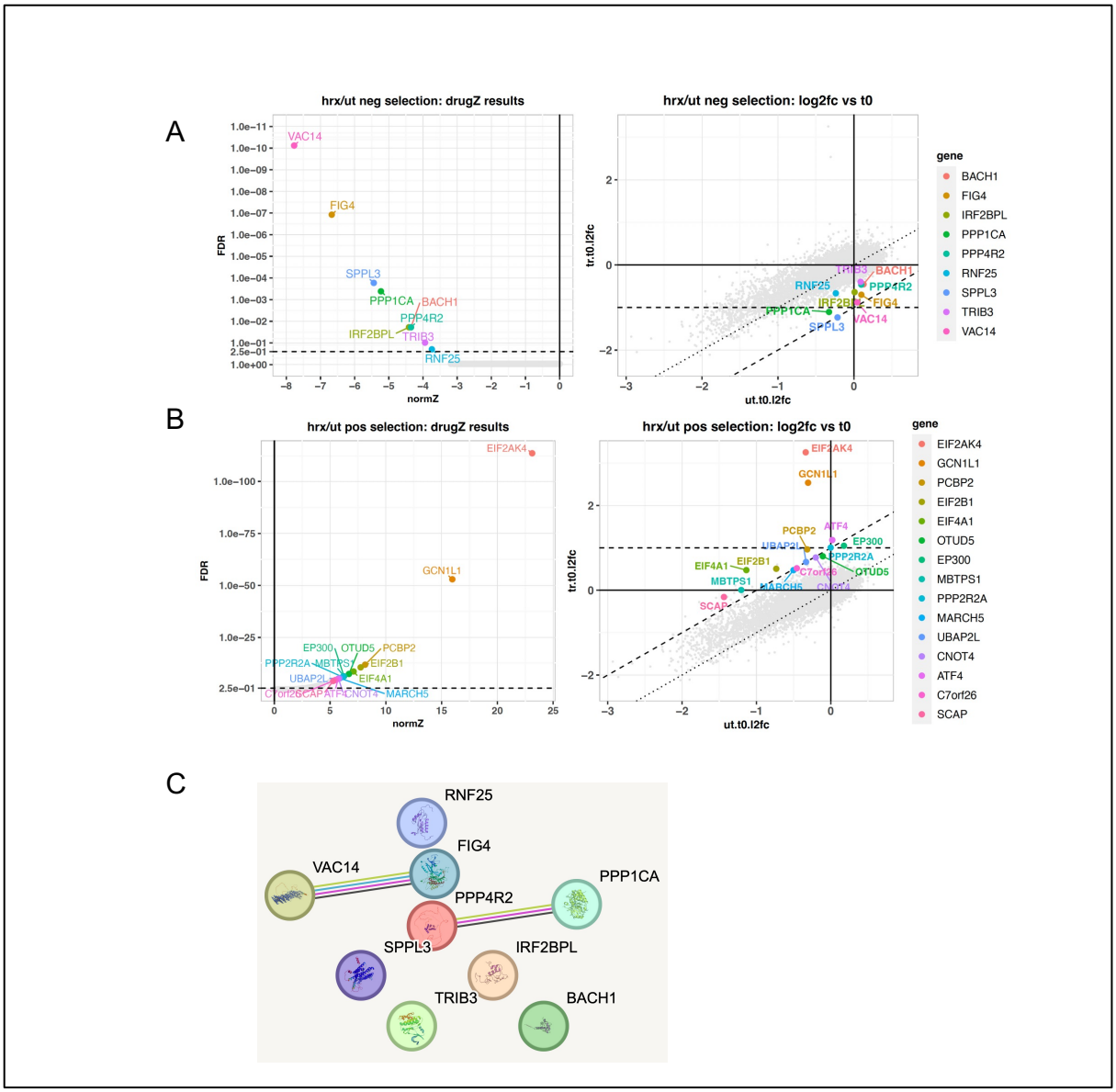

Supplementary figure 5: Genome-wide CRISPR knockout screen in PC3 with HRX-0233. (Left panel) False discovery rate (FDR) of top ranked depleted sgRNAs (A), and of top ranked enriched sgRNAs (B) (Right panel) Volcano plots identified depleted genes of the screen with HRX-0233. X-axis represents log2FC in the untreated condition vs. untreated condition at time point 0 (T=0). Y-Axis represents log2FC in treated condition vs. untreated condition. Log2FC < -1 in treated vs. untreated condition is considered a significant. (C) STRING pathway analysis showing protein-protein association between VAC14 and FIG4, as well as PPP4R2 and PPP1CA.

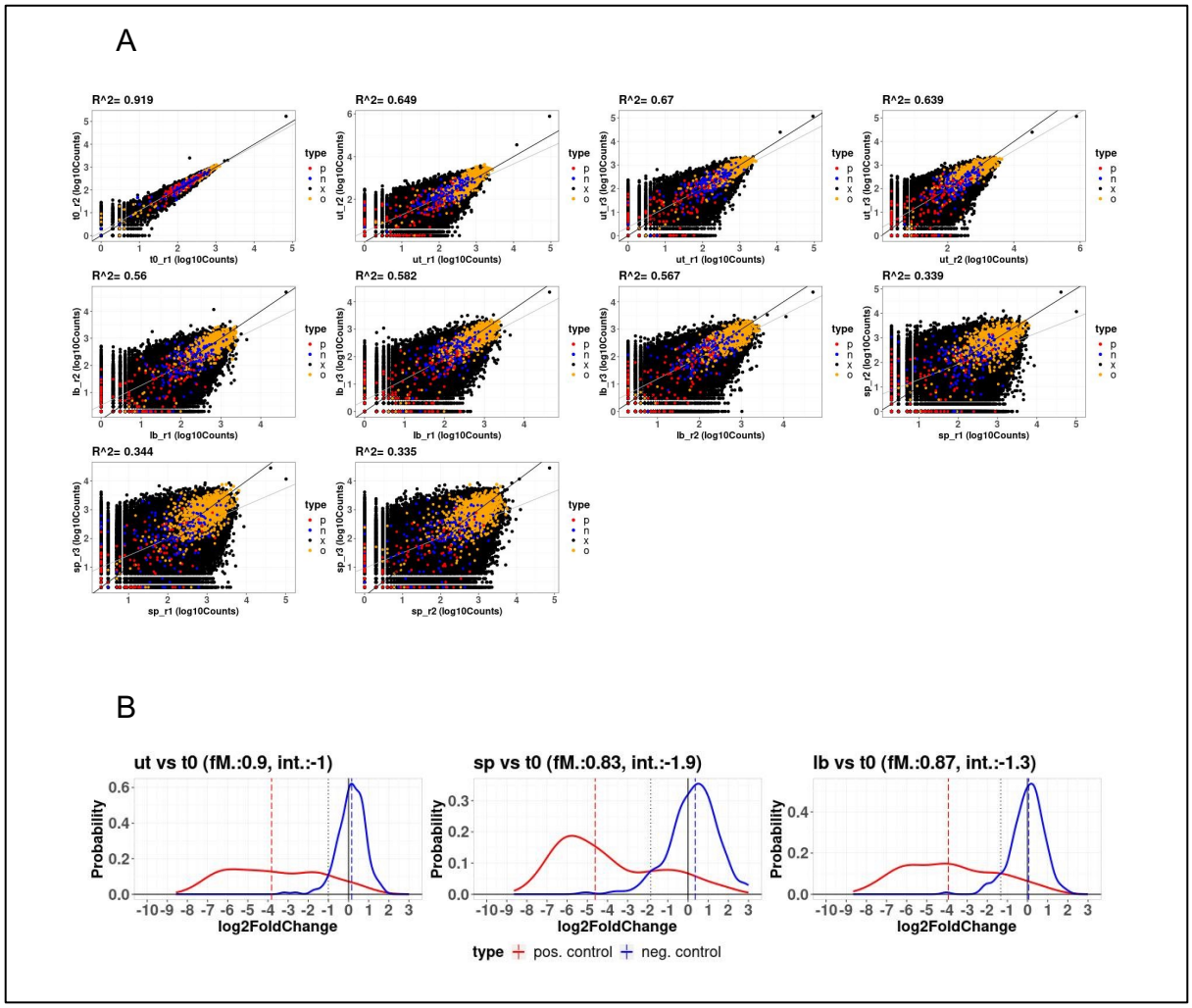

Supplementary figure 6: Quality control of genome-wide CRISPR screen in LnCap-abl cells. (A) Correlation plots of all sgRNA reads between each replicate. (B) Probability distribution of control sgRNAs of each screen condition vs untreated condition at T=0.

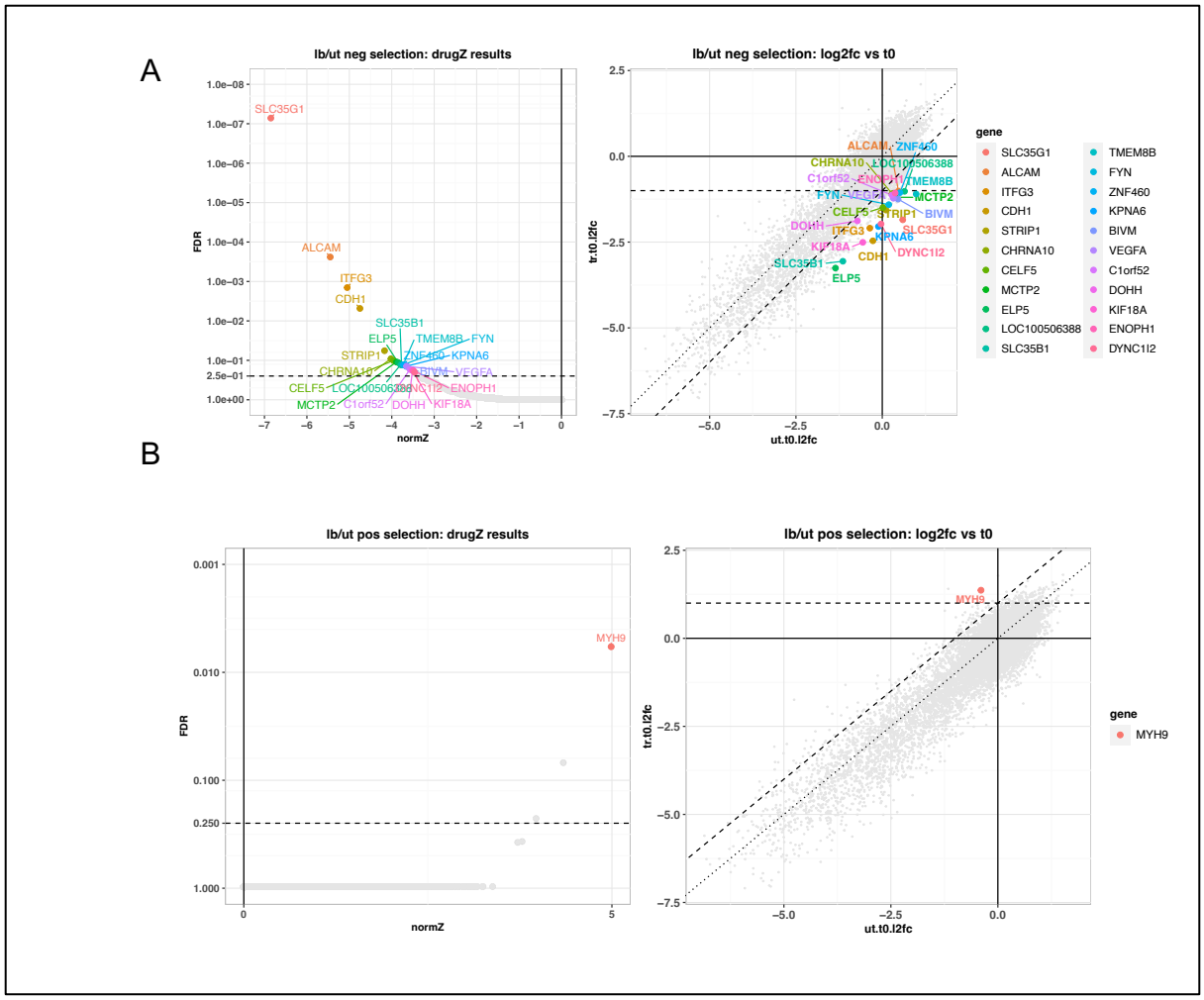

Supplementary figure 7: Genome-wide CRISPR knockout screen in LnCap-abl with LB-100. (A) (Left panel) False discovery rate (FDR) of top ranked depleted sgRNAs and (right panel) volcano plots identified depleted genes. X-axis represents log2FC in the untreated condition vs. untreated condition at time point 0 (T=0). Y-Axis represents log2FC in treated condition vs. untreated condition. Log2FC < -1 in treated vs. untreated condition is considered a significant. (B) (Left panel) False discovery rate of top ranked enriched sgRNAs. (Right panel) Volcano plots identified enriched genes of the screen.

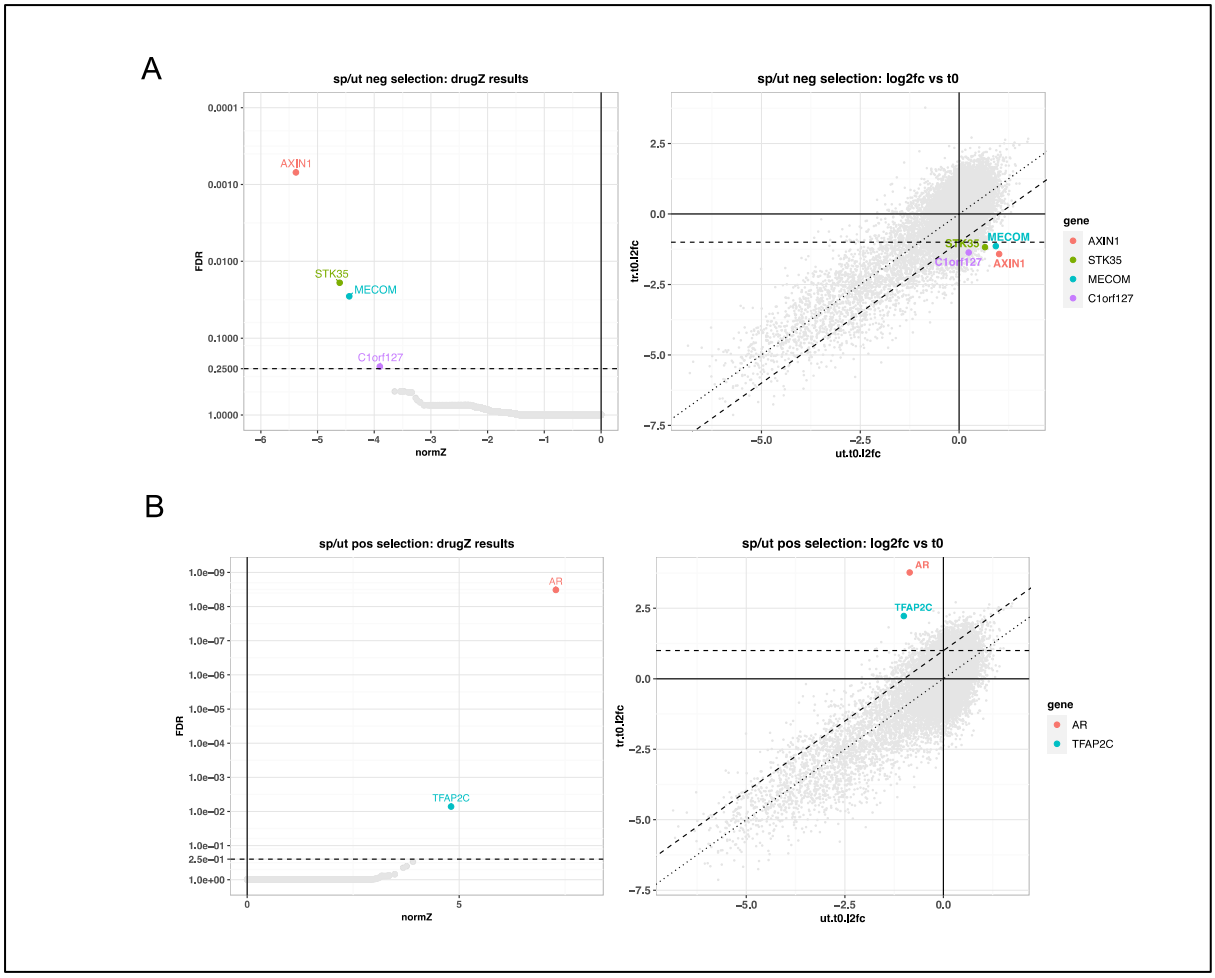

Supplementary figure 8: Genome-wide CRISPR knockout screen in LnCap-abl with R1881. (A) (Left panel) False discovery rate (FDR) of top ranked depleted sgRNAs and (right panel) volcano plots identified depleted genes. X-axis represents log2FC in the untreated condition vs. untreated condition at time point 0 (T=0). Y-Axis represents log2FC in treated condition vs. untreated condition. Log2FC < -1 in treated vs. untreated condition is considered a significant. (B) (Left panel) False discovery rate of top ranked enriched sgRNAs. (Right panel) Volcano plots identified enriched genes of the screen.

8. Acknowledgement

Foremost, I would like to express my heartfelt gratitude to my daily supervisors Koen van der Mijn and Robin Jansen for their exceptional guidance throughout the entire project. Their unwavering support, patience and insightful feedbacks have been instrumental in shaping my understanding and developing my academic skill. This report and the conducted research would never have been possible without them.

I would also like to give special thanks to Professor René Bernards for giving me the invaluable opportunity to delve into this translational field of research, which has enriched my knowledge and opened new horizons for me. His positive attitude and his dedication to cancer research have been a great source of inspiration.

I owe my special thanks to Johan, Elke and Cor, who have generously shared their expertise and helped me to successfully conduct the CRISPR screen experiments that were the major parts of my project. Additionally, I am thankful to Wilbert Zwart, as his provided resources were crucial in realizing the objectives of this study.

My sincere thanks would also go to Katrien, Marielle, Annemiek, Astrid for sharing their research experience and profound suggestions, as they have helped me advance my laboratory and research skills. I would also like to thank Patty for arranging administrative business. I would also like to thank my student peers Eline, Chrysa, Niki, and Lieke for being supportive and encouraging. I cherished memories we have shared together during this journey.

Adiitionally, I would like to thank Prof. Sabine Linn, my examiner, for willing to assess this report.

My gratitude extends to all the members of B7 whose discussions and feedback influenced my thinking and offered fresh perspectives. Scientific discourse thrives in such a community, and I am grateful to be surrounded by such intellectually stimulating individuals. It was a privilege and an honor to work alongside all of you.

On a personal note, I would like to thank my family and friends for their encouragement and understanding. Your belief in me has been a constant source of motivation, and your support propelled me during challenging times.

In conclusion, I am humbled by the collective support, encouragement, and collaboration that have shaped this research endeavor. To everyone who has assisted me along the way, directly or indirectly, in this undertaking, I extend my sincere gratitude.

9. References

[1] Wang, L., Lu, B., He, M., Wang, Y., Wang, Z., & Du, L. (2022). Prostate Cancer Incidence and Mortality: Global Status and Temporal Trends in 89 Countries From 2000 to 2019. Frontiers in public health, 10, 811044. https://doi.org/10.3389/fpubh.2022.811044

[2] Sekhoacha, M., Riet, K., Motloung, P., Gumenku, L., Adegoke, A., & Mashele, S. (2022). Prostate Cancer Review: Genetics, Diagnosis, Treatment Options, and Alternative Approaches. Molecules (Basel, Switzerland), 27(17), 5730. https://doi.org/10.3390/molecules27175730

[3] Carver, B. S., Chapinski, C., Wongvipat, J., Hieronymus, H., Chen, Y., Chandarlapaty, S., Arora, V., Le, C., Koutcher, J. A., Scher, H. I., Scardino, P. T., Rosen, N., & Sawyers, C. L. (2011). Reciprocal feedback regulation of PI3K and androgen receptor signaling in PTEN-Deficient prostate cancer. Cancer Cell, 19(5), 575–586. https://doi.org/10.1016/j.ccr.2011.04.008

[4] Raith F, O'Donovan DH, Lemos C, Politz O, Haendler B. Addressing the Reciprocal Crosstalk between the AR and the PI3K/AKT/mTOR Signaling Pathways for Prostate Cancer Treatment. Int J Mol Sci. 2023 Jan 24;24(3):2289. doi: 10.3390/ijms24032289. PMID: 36768610; PMCID: PMC9917236.

[5] Mulholland, D. J., Tran, L. M., Li, Y., Cai, H., Morim, A., Wang, S., Plaisier, S., Garraway, I. P., Huang, J., Graeber, T. G., & Wu, H. (2011). Cell autonomous role of PTEN in regulating castration-resistant prostate cancer growth. Cancer cell, 19(6), 792–804. https://doi.org/10.1016/j.ccr.2011.05.006

[6] Coleman, N., Moyers, J. T., Harbery, A., Vivanco, I., & Yap, T. A. (2021). Clinical Development of AKT Inhibitors and Associated Predictive Biomarkers to Guide Patient Treatment in Cancer Medicine. Pharmacogenomics and personalized medicine, 14, 1517–1535. doi.org/10.2147/PGPM.S305068

[7] Sweeney, C., Bracarda, S., Sternberg, C. N., Chi, K. N., Olmos, D., Sandhu, S., Massard, C., Matsubara, N., Alekseev, B., Parnis, F., Atduev, V., Buchschacher, G. L., Jr, Gafanov, R., Corrales, L., Borre, M., Stroyakovskiy, D., Alves, G. V., Bournakis, E., Puente, J., Harle-Yge, M. L., … de Bono, J. S. (2021). Ipatasertib plus abiraterone and prednisolone in metastatic castration-resistant prostate cancer (IPATential150): a multicentre, randomised, double-blind, phase 3 trial. Lancet (London, England), 398(10295), 131–142. https://doi.org/10.1016/S0140-6736(21)00580-8

[8] Crabb, S. J., Griffiths, G., Marwood, E., Dunkley, D., Downs, N., Martin, K., Light, M., Northey, J., Wilding, S., Whitehead, A., Shaw, E., Birtle, A. J., Bahl, A., Elliott, T., Westbury, C., Sundar, S., Robinson, A., Jagdev, S., Kumar, S., Rooney, C., … Jones, R. J. (2021). Pan-AKT Inhibitor Capivasertib With Docetaxel and Prednisolone in Metastatic Castration-Resistant Prostate Cancer: A Randomized, Placebo-Controlled Phase II Trial (ProCAID). Journal of clinical oncology : official journal of the American Society of Clinical Oncology, 39(3), 190–201. https://doi.org/10.1200/JCO.20.01576

[9] Regad, T. Targeting RTK Signaling Pathways in Cancer. Cancers 2015, 7, 1758-1784. https://doi.org/10.3390/cancers7030860

[10] Pavese, J., Ogden, I., Voll, E., Huang, X., Xu, L., Jovanovic, B., & Bergan, R. C. (2014). Mitogen-Activated Protein kinase kinase 4 (MAP2K4) promotes human prostate cancer metastasis. PLOS ONE, 9(7), e102289. https://doi.org/10.1371/journal.pone.0102289

[11] Mundt, F., Rajput, S., Li, S., Ruggles, K. V., Mooradian, A. D., Mertins, P., Gillette, M. A., Krug, K., Guo, Z., Hoog, J., Erdmann-Gilmore, P., Primeau, T., Huang, S., Edwards, D. P., Wang, X., Wang, X., Kawaler, E., Mani, D. R., Clauser, K. R., Gao, F., … Ma, C. X. (2018). Mass Spectrometry-Based Proteomics Reveals Potential Roles of NEK9 and MAP2K4 in Resistance to PI3K Inhibition in Triple-Negative Breast Cancers. Cancer research, 78(10), 2732–2746. https://doi.org/10.1158/0008-5472.CAN-17-1990

[12] Dias, M. H., & Bernards, R. (2021). Playing cancer at its own game: activating mitogenic signaling as a paradoxical intervention. Molecular oncology, 15(8), 1975–1985. https://doi.org/10.1002/1878-0261.12979

[13] Sena, L. A., Wang, H., Lim ScM, S. J., Rifkind, I., Ngomba, N., Isaacs, J. T., Luo, J., Pratz, C., Sinibaldi, V., Carducci, M. A., Paller, C. J., Eisenberger, M. A., Markowski, M. C., Antonarakis, E. S., & Denmeade, S. R. (2021). Bipolar androgen therapy sensitizes castration-resistant prostate cancer to subsequent androgen receptor ablative therapy. European journal of cancer (Oxford, England : 1990), 144, 302–309. https://doi.org/10.1016/j.ejca.2020.11.043

[14] Mohammad, O.S.; Nyquist, M.D.; Schweizer, M.T.; Balk, S.P.; Corey, E.; Plymate, S.; Nelson, P.S.; Mostaghel, E.A. Supraphysiologic Testosterone Therapy in the Treatment of Prostate Cancer: Models, Mechanisms and Questions. Cancers 2017, 9, 166. https://doi.org/10.3390/cancers9120166

[15] Guo, H., Wu, Y., Nouri, M. et al. Androgen receptor and MYC equilibration centralizes on developmental super-enhancer. Nat Commun 12, 7308 (2021). https://doi.org/10.1038/s41467-021-27077-y

[16] Ellwood-Yen, K., Graeber, T. G., Wongvipat, J., Iruela-Arispe, M. L., Zhang, J., Matusik, R., Thomas, G. V., & Sawyers, C. L. (2003). Myc-driven murine prostate cancer shares molecular features with human prostate tumors. Cancer cell, 4(3), 223–238. https://doi.org/10.1016/s1535-6108(03)00197-1

[17] Qiu, X., Boufaied, N., Hallal, T. et al. MYC drives aggressive prostate cancer by disrupting transcriptional pause release at androgen receptor targets. Nat Commun 13, 2559 (2022). https://doi.org/10.1038/s41467-022-30257-z

[18] Leone, G., Buttigliero, C., Pisano, C., Di Stefano, R. F., Tabbò, F., Turco, F., Vignani, F., Scagliotti, G. V., Di Maio, M., & Tucci, M. (2020). Bipolar androgen therapy in prostate Cancer: Current evidences and future perspectives. Critical Reviews in Oncology Hematology, 152, 102994. https://doi.org/10.1016/j.critrevonc.2020.102994

[19] Teply, B. A., Wang, H., Luber, B., Sullivan, R., Rifkind, I., Bruns, A., Spitz, A., DeCarli, M., Sinibaldi, V., Pratz, C. F., Lu, C., Silberstein, J. L., Luo, J., Schweizer, M. T., Drake, C. G., Carducci, M. A., Paller, C. J., Antonarakis, E. S., Eisenberger, M. A., & Denmeade, S. R. (2018). Bipolar androgen therapy in men with metastatic castration-resistant prostate cancer after progression on enzalutamide: an open-label, phase 2, multicohort study. The Lancet. Oncology, 19(1), 76–86. https://doi.org/10.1016/S1470-2045(17)30906-3

[20] Schweizer, M. T., Antonarakis, E. S., Wang, H., Ajiboye, A. S., Spitz, A., Cao, H., Luo, J., Haffner, M. C., Yegnasubramanian, S., Carducci, M. A., Eisenberger, M. A., Isaacs, J. T., & Denmeade, S. R. (2015). Effect of bipolar androgen therapy for asymptomatic men with castration-resistant prostate cancer: results from a pilot clinical study. Science translational medicine, 7(269), 269ra2. https://doi.org/10.1126/scitranslmed.3010563

[21] Liu X, Chen X, Rycaj K, Chao HP, Deng Q, Jeter C, Liu C, Honorio S, Li H, David T, Suraneni M, Laffin B, Qin J, et al. Systematic dissecton of phenotypic, functional, and tumorigenic heterogeneity of human prostate cancre cells. Oncotarget. 2015;6:23959-86. doi: 10.18632/oncotarget.4260.

[22] Rycaj K., Cho E., Liu X., Chao H., Liu B., Li Q., Devkota A. K., Zhang D., Chen X., Moore J., Dalby K. N., Tang D. G. Longitudinal tracking of subpopulation dynamics and molecular changes during LNCaP cell castration and identification of inhibitors that could target the PSA−/lo castration-resistant cells. Oncotarget. 2016; 7: 14220-14240. Retrieved from https://www.oncotarget.com/article/7303/text/

[23] Haeusgen, W., Tueffers, L., Herdegen, T., & Waetzig, V. (2014). Map2k4δ - identification and functional characterization of a novel Map2k4 splice variant. Biochimica et biophysica acta, 1843(5), 875–884. https://doi.org/10.1016/j.bbamcr.2014.01.028

[24] Saura, C., Roda, D., Roselló, S., Oliveira, M., Macarulla, T., Pérez-Fidalgo, J. A., Morales-Barrera, R., Sanchis-Garcia, J. M., Musib, L., Budha, N., Zhu, J., Nannini, M., Chan, W. Y., Bohorquez, S. M. S., Meng, R. D., Lin, K., Yan, Y., Patel, P. H., Baselga, J., . . . Cervantes, A. (2017). A First-in-Human Phase I study of the ATP-Competitive AKT inhibitor Ipatasertib demonstrates robust and safe targeting of AKT in patients with solid tumors. Cancer Discovery, 7(1), 102–113. https://doi.org/10.1158/2159-8290.cd-16-0512

[25] Wu, Y. T., Tan, H. L., Huang, Q., Ong, C. N., & Shen, H. M. (2009). Activation of the PI3K-Akt-mTOR signaling pathway promotes necrotic cell death via suppression of autophagy. Autophagy, 5(6), 824–834. https://doi.org/10.4161/auto.9099

[26] Dan, H. C., Ebbs, A., Pasparakis, M., Van Dyke, T., Basseres, D. S., & Baldwin, A. S. (2014). Akt-dependent activation of mTORC1 complex involves phosphorylation of mTOR (mammalian target of rapamycin) by IκB kinase α (IKKα). The Journal of biological chemistry, 289(36), 25227–25240. https://doi.org/10.1074/jbc.M114.554881

[27] Tien, A. H., & Sadar, M. D. (2022). Cyclin-dependent Kinase 4/6 Inhibitor Palbociclib in Combination with Ralaniten Analogs for the Treatment of Androgen Receptor-positive Prostate and Breast Cancers. Molecular cancer therapeutics, 21(2), 294–309. https://doi.org/10.1158/1535-7163.MCT-21-0411

[28 Ren, W., Joshi, R., & Mathew, P. (2016). Synthetic lethality in PTEN-Mutant prostate cancer is induced by combinatorial PI3K/AKT and BCL-XL inhibition. Molecular Cancer Research, 14(12), 1176–1181. https://doi.org/10.1158/1541-7786.mcr-16-0202 https://pubmed.ncbi.nlm.nih.gov/34047239/

[29] Savill, K.M.Z., Lee, B.B., Oeh, J. et al. Distinct resistance mechanisms arise to allosteric vs. ATP-competitive AKT inhibitors. Nat Commun 13, 2057 (2022). https://doi.org/10.1038/s41467-022-29655-0

[30] Leung, J. H., Leung, H. W. C., Wang, S. Y., Huang, S. S., & Chan, A. L. F. (2021). Efficacy and safety of CDK4/6 and PI3K/AKT/mTOR inhibitors as second-line treatment in postmenopausal patients with hormone receptor-positive, HER-2-negative metastatic breast cancer: a network meta-analysis. Expert opinion on drug safety, 20(8), 949–957. https://doi.org/10.1080/14740338.2021.1931116

[31] Xia, Z., Wang, W., Qiu, J., Shi, X., Li, H., Chen, R., Ke, K., Dong, C., Zhu, Y., Wu, S., Zhang, R., Meng, Z., Zhao, H., Gu, P., Leung, K., Wong, M., Liu, X., Zhou, F., Zhang, J., . . . Jiang, B. (2021). Discovery of a New CDK4/6 and PI3K/AKT Multiple Kinase Inhibitor Aminoquinol for the Treatment of Hepatocellular Carcinoma. Frontiers in Pharmacology, 12. https://doi.org/10.3389/fphar.2021.691769

[32] Kase, A. M., Tan, W., Gleba, J., Miller, J. L., Meurice, N., Petit, J., & Copland, J. A. (2022). Patient derived tumor xenograft study with CDK4/6 inhibitor plus AKT inhibitor for management of metastatic castrate resistant prostate cancer. Journal of Clinical Oncology, 40(6_suppl), 176. https://doi.org/10.1200/jco.2022.40.6_suppl.176

[33] Wisdom, R. (1999). C-JUN regulates cell cycle progression and apoptosis by distinct mechanisms. The EMBO Journal, 18(1), 188–197. https://doi.org/10.1093/emboj/18.1.188

[34] Drobnjak, M., Osman, I., Scher, H. I., Fazzari, M., & Cordon-Cardo, C. (2000). Overexpression of cyclin D1 is associated with metastatic prostate cancer to bone. PubMed, 6(5), 1891–1895. https://pubmed.ncbi.nlm.nih.gov/10815912

[35] Qiao, Y., Choi, J. E., Tien, J. C., Simko, S. A., Rajendiran, T., Vo, J. N., Delekta, A. D., Wang, L., Xiao, L., Hodge, N. B., Desai, P., Mendoza, S., Juckette, K., Xu, A., Soni, T., Su, F., Wang, R., Cao, X., Yu, J., Kryczek, I., … Chinnaiyan, A. M. (2021). Autophagy Inhibition by Targeting PIKfyve Potentiates Response to Immune Checkpoint Blockade in Prostate Cancer. Nature cancer, 2, 978–993. https://doi.org/10.1038/s43018-021-00237-1 [36] Qiu, S., Lavallée-Adam, M., & Côté, M. (2021). Proximity Interactome map of the VAC14–FIG4 complex using BioID. Journal of Proteome Research, 20(11), 4959–4973. https://doi.org/10.1021/acs.jproteome.1c00408

[37] Denmeade, S. R., Sena, L. A., Wang, H., Antonarakis, E. S., & Markowski, M. C. (2023). Bipolar Androgen Therapy Followed by Androgen Receptor Inhibition as Sequential Therapy for Prostate Cancer. The oncologist, 28(6), 465–473. https://doi.org/10.1093/oncolo/oyad055

[38] Rodon, J., Dienstmann, R., Serra, V. et al. Development of PI3K inhibitors: lessons learned from early clinical trials. Nat Rev Clin Oncol 10, 143–153 (2013). https://doi.org/10.1038/nrclinonc.2013.10

[39] Deacon K., Blank J.L. Characterization of the mitogen-activated protein kinase kinase 4 (MKK4)/c-Jun NH 2 -terminal kinase 1 and MKK3/p38 pathways regulated by MEK kinases 2 and 3: MEK kinase 3 activates MKK3 but does not cause activation of p38 kinase in vivo. J Biol Chem. 1997;272(22):14489–14496.

[40] Herberts, C., Murtha, A. J., Fu, S., Wang, G., Schönlau, E., Xue, H., Lin, D., Gleave, A., Yip, S., Angeles, A., Hotte, S. J., Tran, B., North, S., Taavitsainen, S., Beja, K., Vandekerkhove, G., Ritch, E., Warner, E. W., Saad, F., . . . Wyatt, A. W. (2020). Activating AKT1 and PIK3CA mutations in metastatic Castration-Resistant prostate cancer. European Urology, 78(6), 834–844. https://doi.org/10.1016/j.eururo.2020.04.058

[41] den Elzen, N., Buttery, C. V., Maddugoda, M. P., Ren, G., & Yap, A. S. (2009). Cadherin adhesion receptors orient the mitotic spindle during symmetric cell division in mammalian epithelia. Molecular biology of the cell, 20(16), 3740–3750. https://doi.org/10.1091/mbc.e09-01-0023

[42] Weaver, L. N., Ems-McClung, S. C., Stout, J. R., LeBlanc, C., Shaw, S. L., Gardner, M. K., & Walczak, C. E. (2011). Kif18A uses a microtubule binding site in the tail for plus-end localization and spindle length regulation. Current biology : CB, 21(17), 1500–1506. https://doi.org/10.1016/j.cub.2011.08.005

[43] Horgan, C. P., Hanscom, S. R., & McCaffrey, M. W. (2011). Dynein LIC1 localizes to the mitotic spindle and midbody and LIC2 localizes to spindle poles during cell division. Cell biology international, 35(2), 171–178. https://doi.org/10.1042/CBI20100284

[44] Vitale, I., Galluzzi, L., Castedo, M., and Kroemer, G. (2011). Mitotic catastrophe: a mechanism for avoiding genomic instability. Nat Rev Mol Cell Biol 12, 385–392. doi:10.1038/nrm3115

[45]Kikuchi A. (1999). Roles of Axin in the Wnt signalling pathway. Cellular signalling, 11(11), 777–788. https://doi.org/10.1016/s0898-6568(99)00054-6

[46] Yardy, G., Bicknell, D., Wilding, J. L., Bartlett, S., Liu, Y., Winney, B., Turner, G. D. H., Brewster, S., & Bodmer, W. F. (2009). Mutations in the AXIN1 gene in advanced prostate cancer. European Urology, 56(3), 486–494. https://doi.org/10.1016/j.eururo.2008.05.029

[47] Otten ABC, Sun BK. Research Techniques Made Simple: CRISPR Genetic Screens. J Invest Dermatol. 2020 Apr;140(4):723-728.e1. doi: 10.1016/j.jid.2020.01.018. PMID: 32200874; PMCID: PMC8525197.

[48] Colic, M., Wang, G., Zimmermann, M. et al. Identifying chemogenetic interactions from CRISPR screens with drugZ. Genome Med 11, 52 (2019). https://doi.org/10.1186/s13073-019-0665-3